Materials and Design 122 (2017) 385–402

Contents lists available at ScienceDirect

Materials and Design

journal homepage: www.elsevier.com/locate/matdes

Effect of incremental equal channel angular pressing (I-ECAP) on the microstructural characteristics and mechanical behaviour of commercially pure titanium

Muhammad Jawad Qarni [a,*], Giribaskar Sivaswamy [a], Andrzej Rosochowski [b], Sonia Boczkal [c]

[a] Advanced Forming Research Centre (AFRC), University of Strathclyde, Inchinnan, Renfrewshire PA4 9LJ, UK
[b] Design Manufacture and Engineering Management (DMEM), University of Strathclyde, Glasgow G1 1XJ, UK
[c] Institute of Non-Ferrous Metals in Gliwice, Light Metals Division, ul. Pilsudskiego 19, 32-050 Skawina, Poland

HIGHLIGHTS

- Commercial purity titanium was processed via incremental equal channel angular pressing at 300 °C.
- The grain refinement achieved was in the ultrafine grain size range and CDRX was a dominant mechanism for grain refinement.
- Significant increase in yield and ultimate tensile strength was achieved with minimal loss of ductility.
- Compression tests at various strain rates reveal a distinct three-stage strain hardening behaviour.
- The processing yielded noticeable increase in hardness characteristics.

GRAPHICAL ABSTRACT

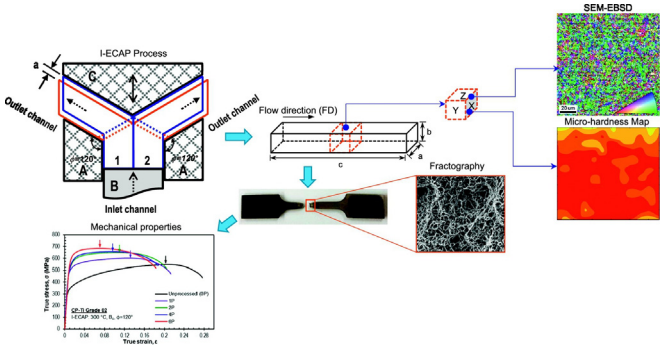

ARTICLE INFO

Article history:
Received 13 December 2016
Received in revised form 16 February 2017
Accepted 5 March 2017
Available online 8 March 2017

Keywords:
Commercially pure titanium
Ultrafine grains (UFG)
Incremental equal channel angular pressing (I-ECAP)
Electron backscatter diffraction (EBSD)
Strain hardening
Microhardness

ABSTRACT

Incremental equal channel angular pressing (I-ECAP) is one of the continuous severe plastic deformation (SPD) processes. This paper presents the processing of commercial purity titanium (CP-Ti) using a double billet variant of I-ECAP process. Ultrafine-grain (UFG) structure was successfully achieved after six passes of I-ECAP at 300 °C. Microstructural evolution and texture development were tracked using EBSD. Analysis revealed continuous dynamic recrystallization (CDRX) as one of the grain refinement mechanism during processing. Room temperature tensile tests carried out before and after six passes, shows significant increase in strength with acceptable levels of ductility. The yield strength was increased from 308 to 558 MPa and ultimate tensile strength from 549 to 685 MPa. Compression tests conducted at different strain rates shows considerable increase in strength and enhanced strain rate sensitivity after processing. A distinct three-stage strain hardening was observed during compression. However the processed material displayed a loss in strain hardening ability during tensile as well as in compression tests. Detailed microhardness measurements show the evolution of hardness after subsequent passes with a reasonable level of homogeneity after the sixth pass. It is demonstrated that I-ECAP is an effective method for grain refinement in CP-Ti and subsequently improving its mechanical properties.

* Corresponding author.
E-mail address: jawad.qarni@strath.ac.uk (M.J. Qarni).

http://dx.doi.org/10.1016/j.matdes.2017.03.015

1. Introduction

Owing to its high specific strength, low density, outstanding corrosion resistance and excellent biocompatibility; titanium is the material of choice in biomedical devices [1,2]. Commercially pure titanium (CP-Ti) is often used in medical implants. However for load bearing joints or total replacement implants, the use of CP-Ti is rather restricted due to its lower strength and therefore Ti-6AL-4V is used instead [3]. Although the addition of alloying elements such as Al and V significantly enhance the mechanical characteristics of titanium, these are considered toxic and therefore undesirable for full bio-integration [4]. An attractive alternative is to improve the mechanical properties of CP-Ti via nano-structuring or grain refinement and therefore the use of these harmful alloying elements can be eliminated altogether. Strengthening of metals via grain refinement has been demonstrated by numerous studies [5,6]. Especially in CP-Ti, after attaining ultrafine grain structure (UFG, grain size less than ~1 μm with high angle grain boundaries), not only improves its yield and tensile strength but also improves the fatigue and corrosion resistance considerably [7,8].

Severe plastic deformation (SPD) is a well-established processing technique for introducing extreme grain refinement and obtaining UFG structure in metals, thereby significantly improving their mechanical properties [9,10]. The process involves imparting large plastic strain in material, without significantly changing the sample dimensions. Several SPD techniques have been developed to date, such as: equal channel angular pressing (ECAP) [11,12], high pressure torsion (HPT) [13], accumulative roll bonding (ARB) [14] etc. All of which have been successfully applied to obtain UFG structure in metals. Among the various techniques available, ECAP is by far the most well studied and widely used technique capable of producing bulk UFG material, large enough for practical applications [15]. Developed by Segal et al. [16], the technique involves passing a billet through a die that consists of two channels with equal cross-sections, intersecting at an angle (Φ) and with an optional outer corner angle (ψ), subtended by the curvature at the outer point of intersection between the two channels. As the billet passes through the intersection, it is subjected to simple shear, while retaining the original cross-sectional area. The billet is normally passed multiple times through the die, in order to impart desired level of plastic strain. The equivalent strain imparted after 'N' number of ECAP passes, can be calculated from Eq. (1) [17].

$$\varepsilon_{eq} = \frac{N}{\sqrt{3}}\left[2\ cot\left(\frac{\phi+\psi}{2}\right) + \psi\ cosec\left(\frac{\phi+\psi}{2}\right)\right] \quad (1)$$

Before the subsequent ECAP pass, the billet is usually rotated along its longitudinal axis, creating different ECAP routes [18,19]. There are four different types of routes; Route A in which the billet is processed repetitively without any rotation, (ii) route B_A in which the billet material is rotated by 90° clock wise and counter clock wise alternatively between consecutive passes (iii) route B_C in which the billet material is rotated by 90° in the same direction between consecutive passes and (iv) route C in which the billet material is rotated by 180° between passes. The distinction between these routes is important, as each route has a different shearing characteristic and therefore each route introduces different shearing pattern which subsequently effects the grain refinement mechanism [20].

Titanium has a hexagonal closed packed (HCP) structure at room temperature and therefore it has a limited number of active dislocation slip systems. This makes it very hard to deform at room temperature as it is susceptible to cracking or failure during processing. To improve the formability of titanium and other such hard to deform materials, ECAP processing is normally carried out at elevated temperature. One of the earliest attempts to establish the workability characteristics of CP-Ti during first pass of ECAP, recommended to use lower processing speed (up to 2.5 mm/s) and higher deformation temperature (between 275 and 325 °C) to avoid failure and segmentation in the processed billets [21].

Several investigations have been performed to refine the grain structure of CP-Ti grade 1 to 4, with the objective of improving the strength characteristics [22–27]. It was established from the data that after multiple passes of ECAP at different die angles (Φ), pressing speeds and temperature conditions, the grain size refinement achieved was in the region of 0.20 to 0.70 μm, with the increase in yield and tensile strength between 1.2 and 2.0 times the original strength. In order to achieve even higher grain refinement, some post deformation have also been applied after ECAP processing. For example Stolyarov et al. [28,29] performed post deformation steps such as cold rolling and cold extrusion on CP-Ti. This yielded significant increase in grain size refinement level through the introduction of more dislocations, this subsequently increased the strength characteristics even further. However, these post deformation steps change the sample dimensions and therefore imposes a limit on the potential usage of material processed. Recently Zhao et al. [30,31] have made successful attempts to process titanium at room temperature to suppress grain growth at higher processing temperature, however these attempts were limited to grade 1 which is considered to be the softest and has the highest formality among commercially available grades of titanium. Using die angles (Φ) of 120° and 90°, it was reported that the grain size reduction achieved at room temperature was between 0.15 and 0.20 μm and the increase in ultimate tensile strength was between 765 and 790 MPa.

From the viewpoint of commercializing UFG materials, recently the interest has been focusing on the continuous SPD methods capable of refining very long or continuous billets. Several techniques have been proposed to transform ECAP into continuous process; such as ECAP conform (ECAP-C) [32], ECAP rolling (ECAR) [33], coshearing [34] and continuous frictional angular extrusion (CFAE) [35]. One such relatively new technique is known as incremental ECAP (I-ECAP), which is capable of processing very long billets.

The purpose of the study is to demonstrate the feasibility of the I-ECAP process for refining the grain structure in CP-Ti with the objective of improving its strength characteristics. The paper includes detailed description about the process and about the experimental setup. CP-Ti grade 2 was subjected to six passes of I-ECAP process at 300 °C. EBSD based inverse pole figure (IPF) maps and pole figures were used to track the grain refinement and deformation characteristics during processing. Tensile tests were performed on samples from subsequent passes, to observe the changes in strength and ductility. Fractography of the tensile samples was performed to investigate the fracture morphology. Compression tests were also performed at various strain rates on unprocessed and severely deformed material to observe the flow stress behaviour in compression and also to evaluate the strain rate sensitivity. Finally, detailed microhardness study was carried out to understand the hardness evolution and to examine the homogeneity of strain distribution during I-ECAP processing.

2. I-ECAP process

In I-ECAP process, the material pressing stage is separated from the deformation stage, as opposed to conventional ECAP where the material pressing and deformation takes place simultaneously. Developed by Rosochowski and Olejnik [36], the process is capable of processing very long or even continuous billets, a distinct advantage over the conventional ECAP. Separating the pressing and deformation stages also facilitate the material flow and reduces pressing force. Thereby, substantially reducing the energy required to carry out the process. I-ECAP can be used for refining grain structures in long bars [37], plates [38] and sheets [39], which makes it an attractive option for industrial implementation.

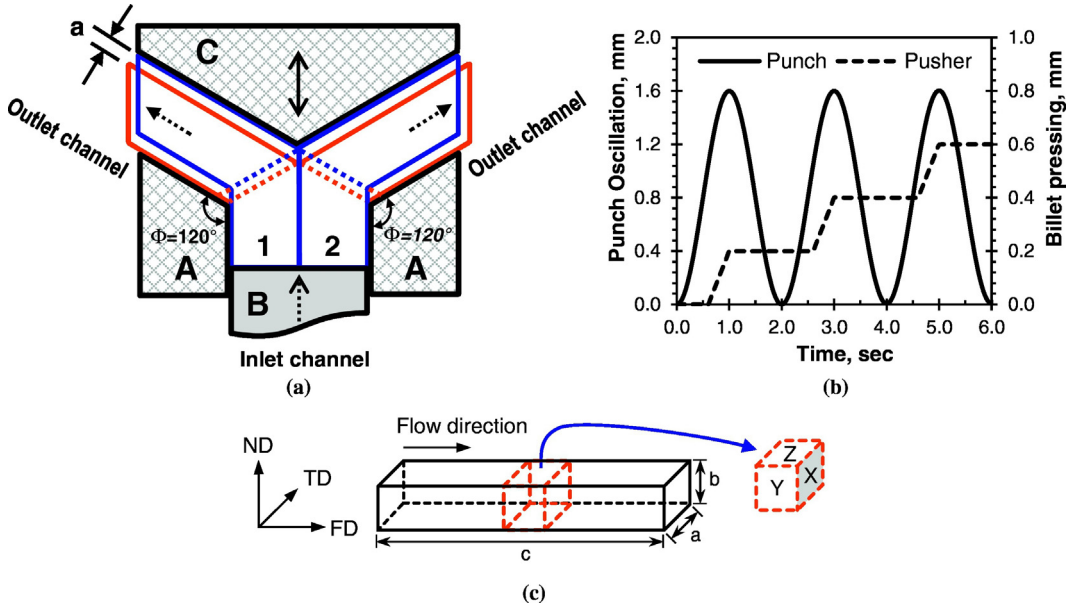

Fig. 1. (a) Schematic illustration of double-billet variant of I-ECAP process (A = Die, B = Plunger and C = Punch), (b) Relative movement of punch and plunger tools during the I-ECAP process and (c) directions of the three orthogonal planes with respect to the billet (FD, ND and TD refers to flow, normal and transverse direction respectively).

2.1. Double billet I-ECAP process

In the present study, the double-billet variant of the I-ECAP process, with a channel intersection angle (Φ) of 120° was used. The schematic illustration of the process is shown in Fig. 1 (a). As the name suggests, the advantage of this variant over the conventional ECAP procedure (other than capability to process longer billets) is that, it can process a two billets simultaneously and therefore has twice the productivity.

There are three main tools; die, plunger and punch denoted by A, B and C respectively in Fig. 1 (a). During the process, the two billets are pushed in an incremental manner by the plunger tool equal to the distance 'a' (shown in Fig. 1 (a)) also known as the pressing stroke; whereas the punch is oscillating at a certain frequency and amplitude. This effectively separates the pressing and the deformation stages. The blue colour outline of the billets in Fig. 1 (a) represents the pressing stage whereas the red colour represents the deformation stage with the dashed outline representing the plastically deformed zone. The mode of deformation is similar to that in classical ECAP process i.e. simple shear, provided the pressing stroke 'a' is not too large. The oscillatory movement of the punch and the incremental movement of the plunger are plotted in Fig. 1 (b) for the first three cycles of the I-ECAP process relative to each other. Fig. 1 (c) defines the representative three orthogonal planes; X, Y and Z with respect to the processed billet. Where X is the cross-sectional or transverse plane perpendicular to the longitudinal axis of the billet and Y and Z plane are the flow and longitudinal planes parallel to the side face and the top face of the billet at the point of exit from the die, respectively [20].

2.2. I-ECAP experimental rig

There are four main elements of the I-ECAP experimental rig; (1) the I-ECAP die, (2) the heating system, (3) the mechanism and (4) the process control system.

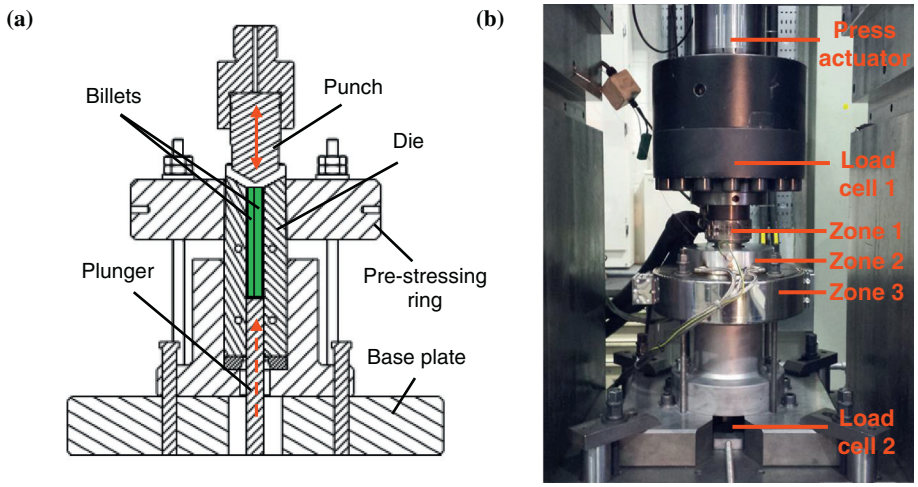

Fig. 2. I-ECAP process (a) CAD drawing of the tool design and (b) actual tooling on 1000 KN hydraulic press.

2.2.1. I-ECAP die

The tool design of the I-ECAP die is shown in Fig. 2 (a), it is comprised of four die inserts assembled together to form the input channel with a pre-stressing ring around the die sub-assembly. The purpose of the pre-stressing ring is to apply high compressive stress in the radial direction and to minimize the tangential stress generated in the die during processing. The punch, die inserts and plunger are all made with a high speed steel alloy heat treated to achieve 60 HRC.

2.2.2. Heating system

In order to avoid cracking and segmentation during processing specially for difficult to deform materials like titanium, the process has to be carried out at elevated temperature. I-ECAP rig consists of three zones of heating as shown in Fig. 2 (b). Zone 1 is a heater band attached to the punch holder with a capacity of 600 W, Zone 2 is a split type aluminum heating block fitted with six fire-rod heaters of 250 W each and finally Zone 3 is a large band heater attached to the pre-stressing ring with a capacity of 3000 W. There is a K-Type thermocouple close to the deformation zone which is used to monitor and maintain the processing temperature within an accuracy of ±2.0 °C during I-ECAP processing.

2.2.3. Mechanism

The I-ECAP process is carried out on a customized 1000 KN servo-hydraulic press (see Fig. 2 (b)) which is controlled by Zwick's Cube controller via Cubus software. In order to realize the I-ECAP mechanism, the punch is coupled to the press actuator and follows a sine wave (oscillatory movements). The plunger tool is connected to a screw jack which is driven by a servo-motor. There are two load cells, one located above the punch (load cell 1 in Fig. 2 (b)) and the other below the plunger tool (load cell 2 in Fig. 2 (b)) to monitor the deformation and pressing forces respectively during processing.

2.2.4. Process control system

To control the pressing of billets and to acquire experimental data during the process, a dedicated LabVIEW virtual instrument application was developed. Fig. 3 (a) shows the national instrumentation chassis and I/O modules which are used to acquire and send signals during experiments. Fig. 3 (b) shows the front screen of this application along with the description of the various controls and display charts. The number on each display chart corresponds to the respective module to which it is connected. The application monitors punch oscillations and based on its position, synchronizes the plunger incremental movements in real time. The billet pressing is accomplished by sending start and stop motion command to the servo motor which drives the screw jack and thereby moving the plunger tool. The application also acquires the pressing as well as deformation forces during processing and records in an Excel file format for post processing purposes.

Table 1
Chemical composition of as received CP-Ti grade 2 material used in this study.

Element	C	N	O	H	Fe	Ti
wt% (max)	0.08	0.03	0.18	0.015	0.20	Balance

3. Material and method

3.1. Material

The as received material used in the present study was commercial purity titanium, grade 2 (here after referred to as CP-Ti) in the form of a 12.5 mm thick hot rolled plate from Dynamic Metals Ltd (UK). The chemical composition of this material is shown in Table 1.

3.2. Billet preparation

Square cross-section billets measuring a = b = 10 mm and c = 120 mm length (a, b and c are indicated in Fig. 1 (c)) were cut using wire electric discharge machining (EDM) such that the length (c) of the billet was parallel to the rolling direction of the plate. A small 1 mm chamfer was machined at the top edge of the billet, to facilitate the flow of material during the initial stage of processing. As titanium is very susceptible to galling on the die walls, therefore it was necessary to perform some steps related to billet preparation prior to I-ECAP experiments. These steps include sandblasting of billets, spray coating a thin layer of lubricant (70% graphite mixed with 30% water) on the billets, drying in the oven at 100 °C and finally applying a thin coating of anti-seize lubricant Loctite 8009 from Henkel Ltd. This method of billet preparation and lubrication was the most effective to avoid any billet seizing during operation. The appearance of billet after different preparatory steps is shown in Fig. 4.

3.3. Experimental procedure

Before starting the I-ECAP experiments, the pair of lubricated billets was left inside the die pre-heated to 300 °C for 15 min, in order to achieve homogenous temperature within the billets. Experiments were performed using a feed rate of 0.2 mm/cycle (0.1 mm/s), punch oscillatory movement of 0.5 Hz with a peak to peak amplitude of 1.6 mm. The die configuration lead to an imposed strain of ~0.67 per pass through the I-ECAP die. The billets were processed repeatedly and were subjected to a total of six passes giving a maximum strain of ~4.02. Processing route B_C was followed in which the billet is rotated by 90° about its longitudinal axis in the same direction after each pass.

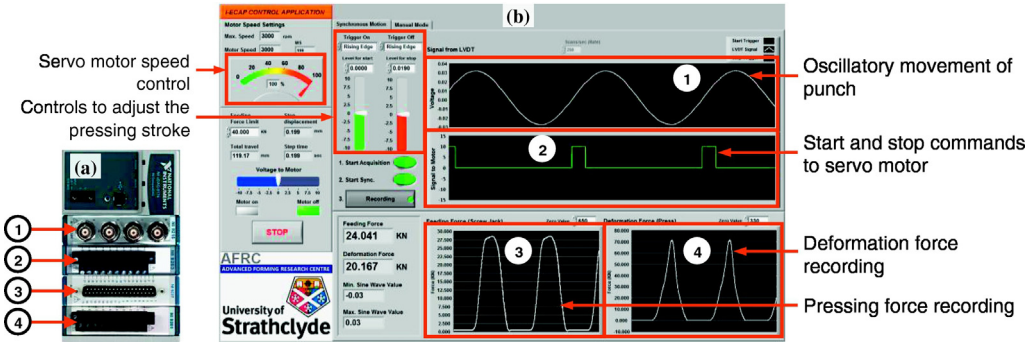

Fig. 3. (a) National instruments chassis along with the four I/O modules for data acquisition and (b) front screen of the LabVIEW virtual instrument application used to monitor, control and acquire data during the I-ECAP experiments (the numbering on the chart corresponds to the respective I/O module to which it is connected).

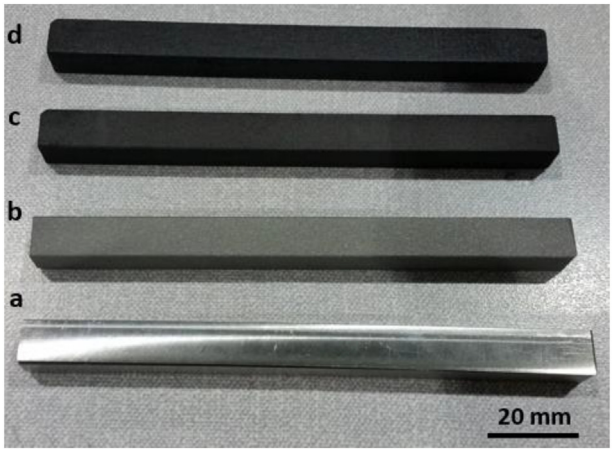

Fig. 4. Billet appearance after different steps of billet preparation (a) 1st step – initial machined billet, (b) 2nd step – sand blasted billet, (c) 3rd step – graphite coated billet and (d) 4th step – anti-seize lubricant applied.

Route B_C is considered to be the most effective in achieving homogenous microstructure in which grains are separated by high angle boundaries [17]. Compared to other routes, route B_C in Ti yields finer equiaxed grains, produces better surface quality billets [40] and also superior corrosion resistance [41]. Following each pass, in order to suppress grain growth, the billets were quenched in cold water and taken to room temperature quickly.

3.4. Mechanical testing and microstructure characterization

Tensile tests were carried out following the ASTM E8 standard, to evaluate the strength and ductility of the material in the unprocessed condition (0P) and after first (1P), second (2P), fourth (4P) and sixth (6P) passes of the I-ECAP. For this purpose, flat tensile sample with a 14 mm gauge length, 3×2 mm^2 cross-section (see Fig. 5 (a) for detailed dimensions), were cut parallel to longitudinal axis (Y plane) of the processed billet using 0.5 mm wire EDM. A set of three samples were cut from each billet across the width (w). To avoid the effect of any surface defect, the samples were cut 1 mm away from the side faces (see Fig. 5 (b) for illustration). All tests were performed at room temperature, at a constant strain rate ($\dot{\varepsilon}$) of 0.01 s^{-1} and taken up to fracture using the Zwick/Roell Z150 test machine with testXpert control software. The load-displacement data from each test was converted into true stress-strain curve. For each material condition, three separate tests were performed to ensure repeatability and the final stress-strain curve for each condition represents the average of the three tests. Following the tensile testing, fracture surface of the samples was examined to study the fracture morphology, using the FEI's Quanta FEG 250 scanning electron microscope (SEM), operating at 20 kV and with secondary electron (SE) mode.

In order to study the effect of I-ECAP processing on the compression behaviour of CP-Ti, uniaxial compression tests were performed on the unprocessed condition and after six passes. Cylindrical samples measuring diameter (ø) = 8 mm and height (h) = 8 mm were machined, such that the axis of each sample was along the longitudinal axis of billet. To minimize the barrelling of samples and to reduce the effect of friction during the test, the top and bottom surface of the samples were coated with molybdenum-disulphide (MoS_2) and the punch surfaces were coated with a thin layer of boron nitride. Using the Zwick HA250 hydraulic machine with a 250 KN load cell, the samples were deformed to achieve 50% height reduction. The tests were performed at 0.01, 0.1 and 1.0 s^{-1} to evaluate the strain rate sensitivity.

Electron back scatter diffraction (EBSD) was used to characterize the microstructure in the unprocessed condition and after subsequent passes of I-ECAP. For characterization purposes, slice of material was cut from the middle of billet to avoid end effects. The surface of the sample was polished using standard mechanical polishing techniques and was then ion milled on Leica RES101 as a final step. The SEM used was a FEI Inspect F50 with an EDAX TSL EBSD detector. The sample was tilted 70° from the horizontal for EBSD data collection, at a 20 kV accelerating voltage and 200 mA beam current. A step size of 0.40 μm was used for the unprocessed material and 80 nm for the sixth pass processed material. Analysis of the EBSD data was performed using TSL OIM software.

Finally, hardness measurements were performed to investigate the evolution of hardness and to examine the homogeneity of strain distribution during I-ECAP processing. Samples measuring 10 mm in thickness, were cut from the centre of the unprocessed billet and from first, second, fourth and sixth pass billets across the transverse (X) plane. Each sample was then mounted and polished to a mirror-like finish using 600, 1200, 2500 and 4000 grit SiC papers. Vicker micro-hardness (Hv) measurements were taken on the surface of each sample using Zwick ZHVμ micro hardness tester equipped with Vickers indenter. For each measurement, a load of 1000 gf was applied for a dwell time of 10 s. The measurements were taken on a 2D grid style pattern of 11×11 equi-spaced points (as shown in Fig. 5 (c)) along TD and ND directions respectively, after leaving a gap of 0.5 mm from all four sides walls. This resulted in a total of 122 measurement points across the sample surface. A detailed contour map was subsequently generated representing the hardness distribution profile for each sample condition.

4. Results and discussion

4.1. Appearance of billets

In Fig. 6 (a) the pair of CP-Ti billets can be seen emerging out of the I-ECAP die at the end of the first pass. The process uniformly deformed billets and the macroscopic appearance of the processed billets was smooth with no signs of defects or surface cracks. The processed billets however exhibited slight bowing, which prevented the pair of billet to be re-inserted in the inlet channel for next pass. Therefore, a secondary straightening operation was performed by pressing the pair of billets on a 5000 KN hydraulic press between two flat dies heated at 200 °C. The Fig. 6 (b) shows the appearance of the billets at different stages: unprocessed billet before I-ECAP (bottom), after I-ECAP (middle) and after straightening operation (top).

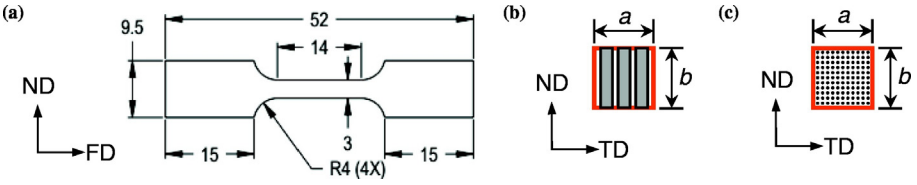

Fig. 5. (a) Dimensions of the flat tensile sample used in this study, (b) illustration of the three tensile samples cut across the cross-section (X-plane) of the billet and (c) 2D grid style pattern of 11×11 equi-spaced points on the surface of the sample used for microhardness measurement study.

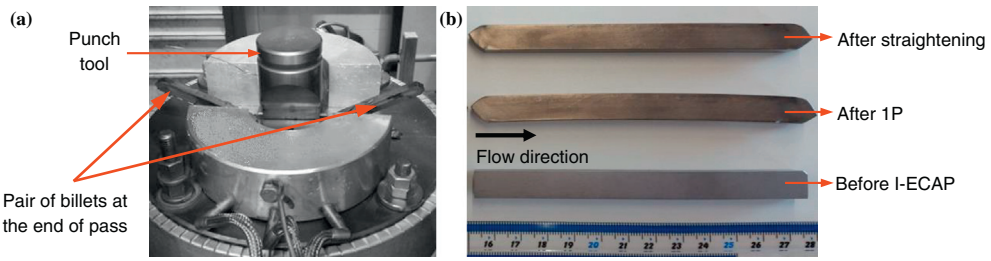

Fig. 6. (a) The pair of CP-Ti billets can be seen emerging out at the end of first I-ECAP pass, (b) Appearance of the CP-Ti billets, unprocessed billet (bottom), billet after first pass of I-ECAP process showing bowing (middle) and straightened billet after secondary operation (top).

4.2. Loads during processing

Fig. 7 (a–f) represent the graphs showing recorded forces on punch and plunger tool, also known as deformation and pressing forces respectively; during the (a) first, (b) second, (c) third, (d) fourth, (e) fifth and (f) sixth pass of I-ECAP. The Y-axis of the graphs represents force in KN and X-axis represents the stroke length. Note that the overall stroke is 10 mm less than the actual billet length, this is to prevent flattening of the tail. For better visualization, the recorded data was sampled and is presented such that, the forces only represent every 25th cycle during each pass. Due to the cyclic nature of the I-ECAP process, both the deformation and pressing forces rises to a peak value and then falls to lower value. During the initial stage of processing the deformation force in all passes can be seen to increase up to a certain stroke length, beyond which it becomes somewhat uniform. This stage of force increase is mainly due to the gradual increase in the contact area between the oscillating punch and the billet top surface (parallel to Z plane). Once there is full contact between the punch surface and billet surface, the force becomes uniform. Moreover, the deformation force is also seen to increase after subsequent passes. As shown in Fig. 8 (a), the maximum values of force required to deform the pair of billets, progressively increased from 68.8 KN during the first pass to 92.5 KN in the

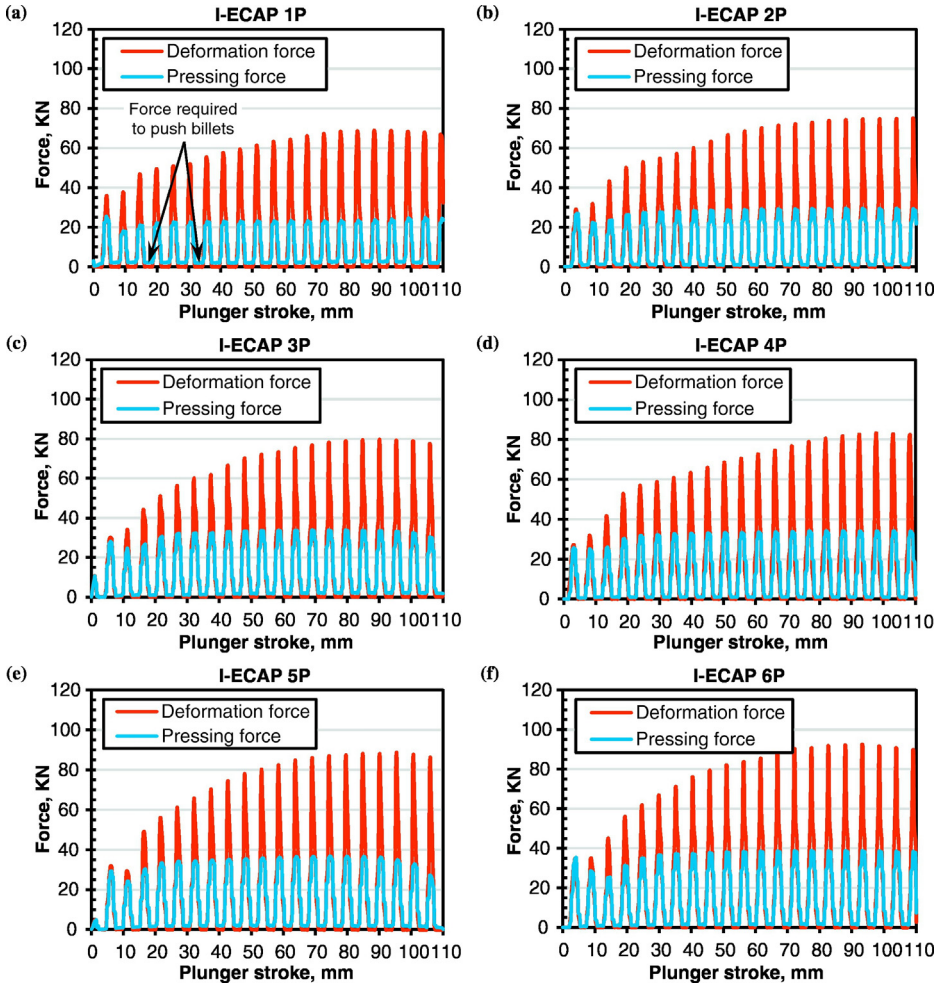

Fig. 7. Deformation and pressing forces recorded during (a) first pass, (b) second pass, (c) third pass, (d) fourth pass, (e) fifth pass and (f) sixth pass of I-ECAP processing.

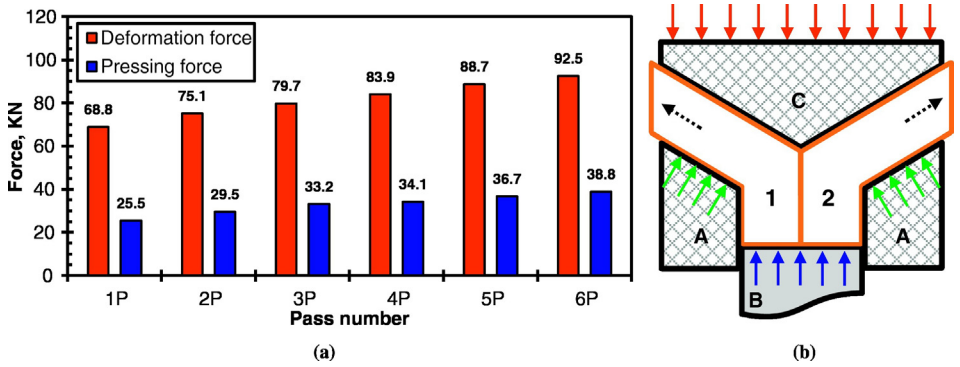

Fig. 8. (a) Values of maximum deformation and pressing forces during different passes of I-ECAP and (b) illustration of load distribution during the deformation stage. (For interpretation of the references to color in this figure, the reader is referred to the web version of this article.)

sixth pass. This strongly suggests that the strength of billets is increasing after each pass and therefore greater force is required to deform the billets.

In Fig. 7 (a–f), the peak values of pressing force during any cycle represent the force required to support the billets during deformation stages. This is illustrated in the Fig. 8 (b), the red arrows indicate force applied by punch C to deform the pair of billets, this load is counter balanced not only by the die A (shown as green arrows) but also by the plunger B (shown as blue arrows). The actual force required to push the pair of billets during the pressing stage is between 1–3 KN (indicated by arrows in Fig. 7 (a)), so small that it is hardly visible in the graphs.

Studies [42,43] have shown that the contact friction during ECAP plays a critical role with respect to homogenous deformation and good surface quality in billet. It is desirable to reduce the contact friction during processing to facilitate optimum processing conditions. However in classical ECAP, it is challenging to provide low friction especially along the bottom wall of the exit channel due to high contact pressure and lubricant removal during processing [42]. The load on plunger is mainly dependent on the material shear flow stress, die configuration, billet shape and friction. When a single lubricated billet is processed through a fixed ECAP die, contact friction is present on almost all surfaces of the billet during processing. This contact area increases with increase in billet length. Therefore, the force required to carry out ECAP process not only increases when processing higher strength materials but also increases when the billet length is increased. Consequently, in order to prevent the load on plunger not to exceed beyond its yield strength, the billet length to width (c/a) ratio is normally limited to 6–10. Thereby limiting the capability of ECAP to process longer billets. I-ECAP method was developed to eliminate this limitation of ECAP. As demonstrated by Fig. 7 (a–f), the actual pressing force required to carry out the process is very small. Thus I-ECAP enables processing of very long or continuous billets.

4.3. Microstructure observations

To understand the level of grain refinement and the deformation characteristics during I-ECAP process, the microstructure and the texture of the CP-Ti before and after subsequent I-ECAP processing was analysed using SEM based EBSD technique. Fig. 9 shows the coloured inverse pole figure (IPF) map of the unprocessed (0P) material. The RGB colour code: red for {0 0 0 1}, green for {2 $\bar{1}$ $\bar{1}$ 0} and blue for {1 0 $\bar{1}$ 0} as shown in the standard stereographic triangle; corresponds to the crystallographic orientation of each grain. The colour variations within the grains qualitatively represent difference in internal misorientations. Fig. 9 also shows the texture represented by the (0 0 0 1) pole figure which was recorded at the same measurement location as the IPF map.

The microstructure of the unprocessed material in Fig. 9 shows the presence of grains which are predominantly equi-axed in morphology. Some small grains are observed within the matrix of pre-existing grains and a few of them are also seen around the boundaries of large grains. Many grains are showing minor misorientation difference within the grain interiors as well. The average grain size was 22 μm obtained from the grain size analysis. The estimated texture shows that the

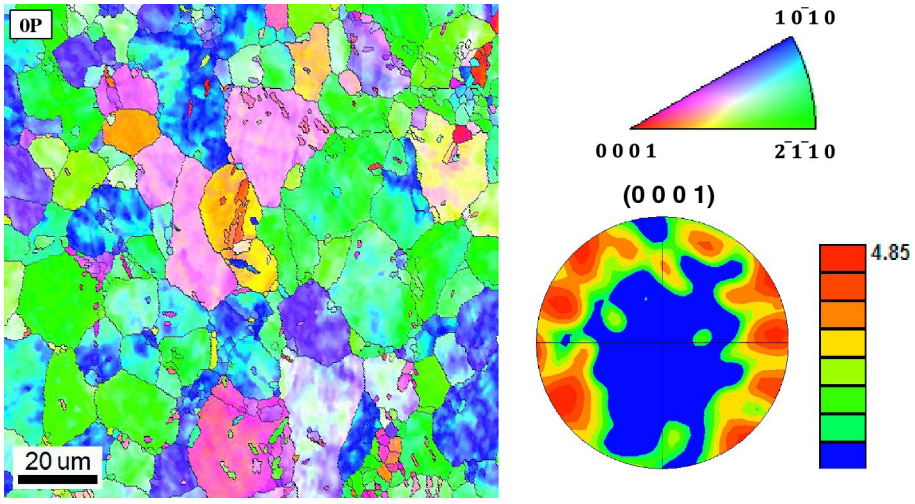

Fig. 9. Inverse pole figure (IPF) maps obtained from EBSD analysis showing the microstructure of unprocessed CP-Ti samples (colour coding is shown in the standard stereographic triangle) and the corresponding (0 0 0 1) pole figure. (For interpretation of the references to color in this figure legend, the reader is referred to the web version of this article.)

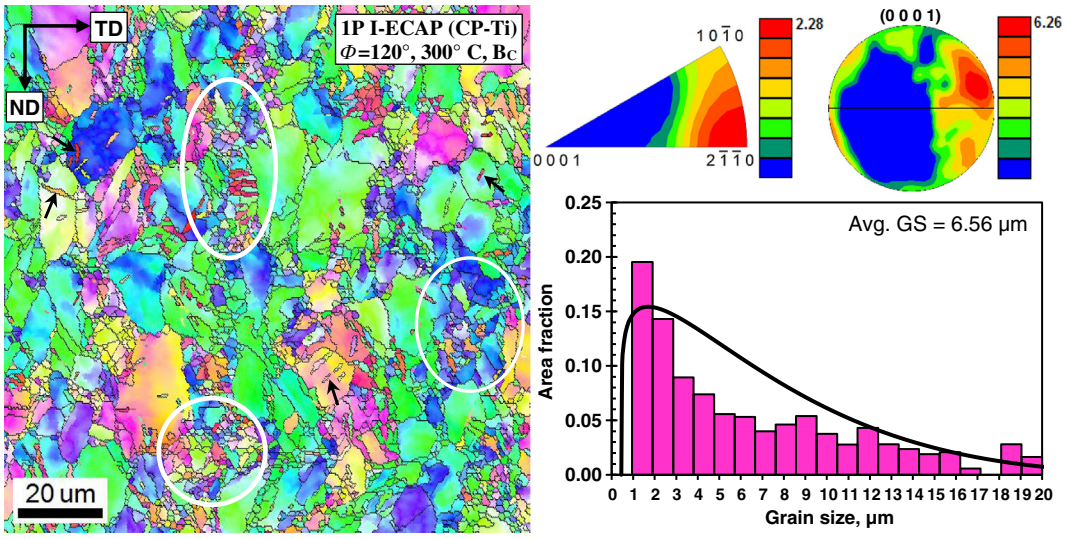

Fig. 10. EBSD based IPF map after first pass of I-ECAP process along with the associated inverse pole figure and the (0 0 0 1) pole figure. The figure also shows grain size histogram.

basal plane of the grains are preferentially oriented parallel to the rolling direction. As a result, a ring texture forms in the pole figure in which the intensity of the basal pole densities are distributed 360° non-uniformly at the periphery of the pole figure.

Figs. 10 to 13, shows the IPF maps representing the post deformation microstructural characteristics along the transverse (X) plane of the samples after first, second, fourth and sixth pass of I-ECAP process, respectively. The figures also include the corresponding inverse pole figures, pole figures along (0 0 0 1) plane and grain size histogram with beta density distribution function. The texture represented by the pole figures were recorded on the samples at the same measurement areas as used for the IPF maps. It is also important to emphasize that the samples for EBSD analysis were taken from the centre region of the processed billets to avoid any end effects and surface defects due to friction.

The IPF map of the sample subjected to first pass of I-ECAP, given in Fig. 10 shows grain refinement in action. Evidence of which is seen by the formation of fine grains which are seen in small clusters at various regions (marked by white circles) within the scanned area. The fine grains are also observed along the boundaries of large grains, forming a so-called necklace structure. These fine grains (below 2 μm) comprise of ~20% of the scanned area fraction. The average grain size based on the grain size histogram after first pass is 6.56 μm, a refinement of ~70% compared to the unprocessed material. Notice that there is no tilt in the metal flow, this is a characteristic feature of the shearing process along transverse (X) plane during first pass of ECAP, as illustrated in Table 2 by Furukawa et al. [19]. In general, the microstructure consists of mostly equi-axed large and fine grains. However, there is some presence of elongated grains in the microstructure as well. Moreover, evidence of some twin formation is also seen in the microstructure, as indicated by black arrows. Titanium has a HCP crystal structure and therefore compared to FCC and BCC, it is expected to behave differently under shear deformation. In cubic metals, deformation is predominately by slip whereas in titanium which has a limited number of slip systems, twinning always play a critical role in the plastic deformation [44]. Several studies have confirmed presence of twinning during ECAP of CP-Ti, it was reported that twinning plays a key role as a mechanism of grain refinement [45,46]. After the first pass, the microstructure can therefore be regarded as highly heterogeneous (anisotropic), because it consists of a mixture of large grains, fine grains and twins after the first pass processing. This heterogeneity in the microstructure after first pass processing in CP-Ti is consistent with other similar studies [45,47]. The pole figure shows that texture intensity has increased from 4.85 to

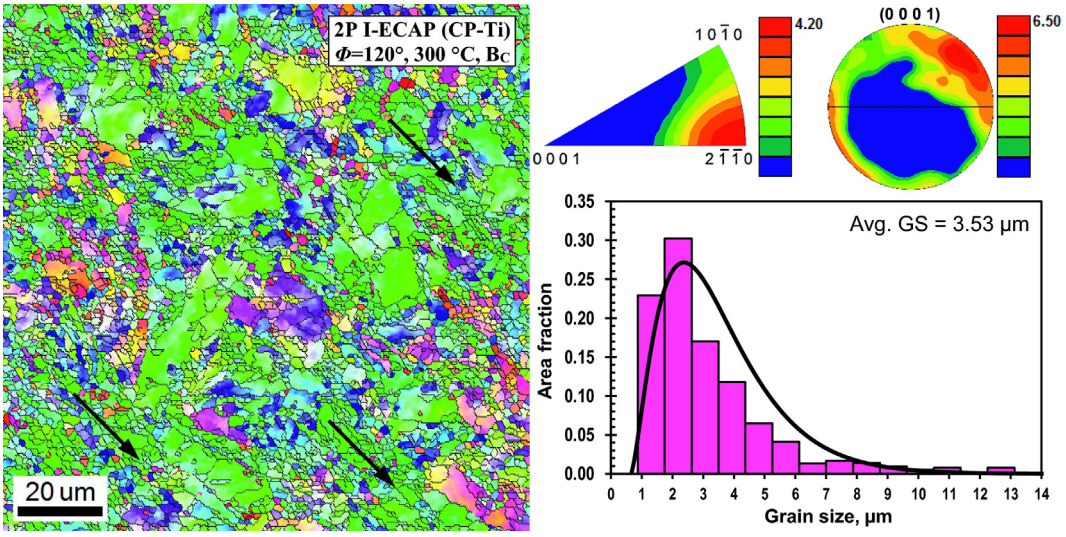

Fig. 11. EBSD based IPF map after second pass of I-ECAP process along with the associated inverse pole figure and the (0 0 0 1) pole figure. The figure also shows grain size histogram.

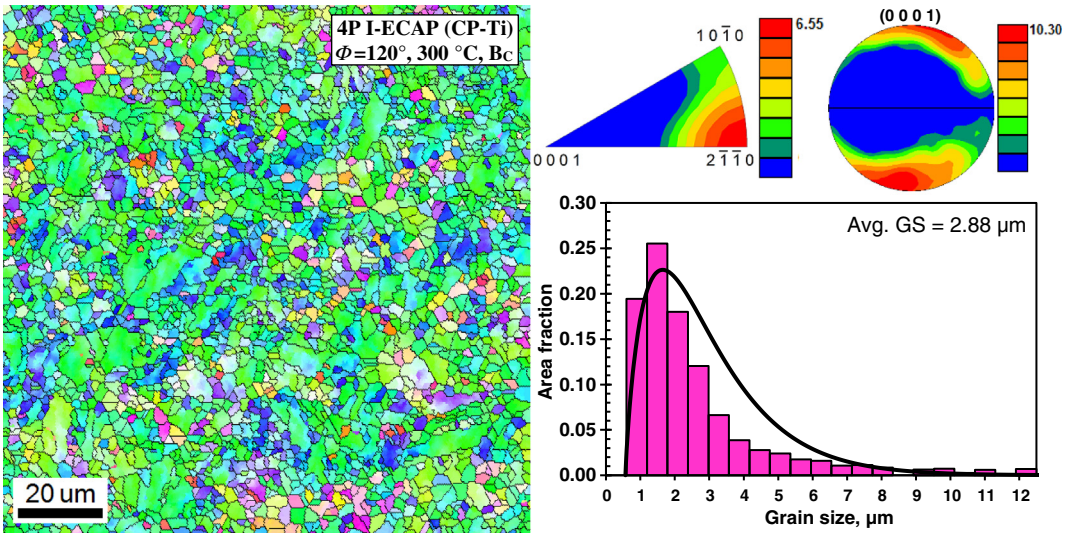

Fig. 12. EBSD based IPF map after fourth pass of I-ECAP process along with the associated inverse pole figure and the (0 0 0 1) pole figure. The figure also shows grain size histogram.

6.26. This is also supported with the inverse pole figure, which reveals that most of the grains have an orientation towards the 2 $\bar{1}$ $\bar{1}$ 0. The inverse pole figure also shows evidence for the development of fibre texture {2 $\bar{1}$ $\bar{1}$ 0} ⟨10 $\bar{1}$ 0⟩ between the positions 1 0 $\bar{1}$ 0 and 2 $\bar{1}$ $\bar{1}$ 0.

Fig. 11 represents the microstructure and the texture after second pass of I-ECAP. It is evident that significant grain refinement has taken place and the average grain size is down to 3.59 μm. The majority of the grains are now fine and equi-axed in morphology. The grain refinement has contributed in the reduction in twin fraction, compared to the first pass. It is widely reported that the twinning activity in titanium is strongly dependent on the grain size, it decreases with reduction in grain size [48]. Overall, the heterogeneity of the microstructure has been reduced considerably. The grain size histogram also shows that the bars have moved to the left side i.e. towards the smaller grain size values. Moreover, the metal flow is seen at a tilt (shown by the direction of arrows) consistent to second pass ECAP processing along transverse (X) plane via route B_C. Increase in the intensity values associated with pole and inverse pole figures confirmed further strengthening of texture compared to first pass.

The IPF map in Fig. 12 represents the microstructural state after fourth pass, which is remarkably different from the first pass processing. Further grain refinement has taken place and some large grains seen in the second pass has been broken into finer grains. The microstructure is homogenous and is dominated by these fine equi-axed grains with ~85% of the grains below 4 μm size. Pole figures and inverse pole figures after fourth pass show significant increase in the texture strength. However, the fibre texture {2 $\bar{1}$ $\bar{1}$ 0} ⟨10 $\bar{1}$ 0⟩ is still between the positions 1 0 $\bar{1}$ 0 and 2 $\bar{1}$ $\bar{1}$ 0.

The EBSD map of the sample after sixth pass in Fig. 13 shows extraordinary level of grain refinement. More than 80% of the grains shown in the scanned area are below submicron range. The microstructure is homogenous and heterogeneity has been completely lost. The average grain size after six pass is 0.89 μm. Fibre texture started to concentrate more towards 2 $\bar{1}$ $\bar{1}$ 0 position in the inverse pole figure. Evidence for the development of a new fibre at around 10° from 0 0 0 1 position is also observed. This has contributed to weakening of texture strength occurs after sixth pass.

Titanium is a high stacking fault energy (SFE) metal and is expected to exhibit continuous dynamic recrystallization (CDRX) during elevated temperature deformation processes. Recent studies on ECAP of CP-Ti have reported CDRX as one of the grain refinement mechanism [49, 50]. CDRX is a recovery dominated process whereby progressive

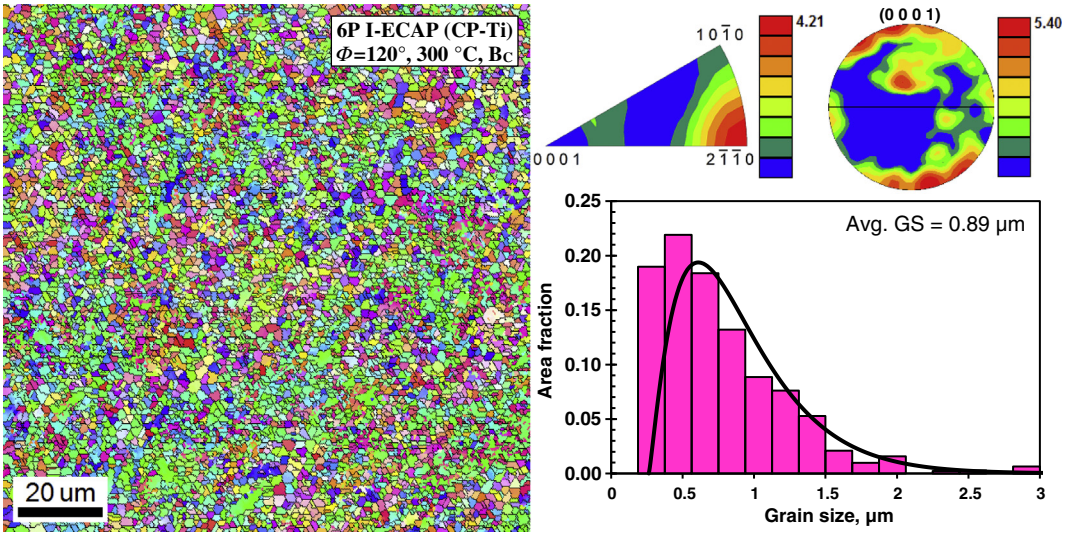

Fig. 13. EBSD based IPF map after sixth pass of I-ECAP process along with the associated inverse pole figure and the (0 0 0 1) pole figure. The figure also shows grain size histogram.

Table 2
Summary of I-ECAP processing parameters used in the study.

No.	Variable	Category	Value	Unit
1	Channel intersection angle (ϕ)	Geometry	120	° (deg)
2	Outer corner angle (ψ)		0	° (deg)
3	Temperature	Processing conditions	300	°C
4	Processing route		B_C	–
5	No. of passes		6	–
6	I-ECAP variant	I-ECAP parameters	Double billet	–
7	Frequency of punch oscillation		0.5	Hz
8	Amplitude of punch oscillation		1.6 (peak to peak)	mm
9	Pressing speed (plunger increments)		0.2 (0.1)	mm/cycle (mm/s)

absorption of dislocations within grains near grain boundaries generates subgrains with low angle grains boundaries (LAGB) [51]. Upon further straining the material, the subgrains continue to rotate and the misorientations (θ) around the LAGBs continue to increase. Consequently, when the misorientation reaches the LAGB/HAGB cut-off (15°) value, new fine grains are originated with high angle grain boundaries (HAGB).

To observe CDRX in the present study, a high magnification EBSD map is generated from the second pass sample, shown in Fig. 14. In the EBSD map, the thin blue lines represent the LAGBs with θ between 2 and 15°, whereas the thick red lines represent the HAGBs with $\theta > 15°$. Incomplete HAGB segments (indicated by black arrow) which do not form a fully enclosed grain are found throughout the scanned area. These incomplete HAGB segments are a strong indication of the CDRX process. The incomplete HAGBs have evolved from the LAGBs, by the progressive accumulations of the dislocations near the boundaries. Careful analysis of two of these incomplete HAGBs, labelled as L1 and L2 reveals that the misorientation is just over 15° (see the corresponding graphs in Fig. 14). This confirm that these HAGBs have evolved from LAGBs. Further dislocation absorption in subsequent passes will lead to the extension of these incomplete HAGBs segments to form fully enclose refined grains. Another characteristic feature associated with CDRX is the formation of necklace structure, i.e. fine grains decorated around the coarse grains [52]. Fig. 14 also shows that most of the LAGBs (subgrains) development is around HAGBs. Since existing HAGBs act as nucleating sites for subgrains, it is expected that the grain refinement takes place at the exterior of coarse grains and spreads towards grain interior [49].

4.4. Mechanical properties

4.4.1. Tensile properties

Fig. 15 (a) shows the fractured tensile samples, after the room temperature tensile tests conducted at constant strain rate ($\dot{\varepsilon}$) of 0.01 s^{-1} for the unprocessed condition and for first, second, fourth and sixth pass of I-ECAP. Fig. 15 (b) shows the corresponding true stress-strain curves obtained from the tensile testing. The unprocessed material shows significant strain hardening beyond the yield point. For the processed material, it is seen that the level of yield strength (0.2% proof stress, σ_y) and ultimate tensile strength (σ_{UTS}) is greatly enhanced after the first pass and second pass compared to the unprocessed material. Although the level of strengthening is somewhat lower between second and fourth pass, this level improves again between fourth to sixth pass. Overall, it is apparent that the strength characteristic is gradually increasing due to the grain refinement taking place after each pass. In general, six passes of I-ECAP processing led to a significant increase in the values of yield strength and ultimate tensile strength in CP-Ti.

Table 3 shows the individual values of strength and elongation derived from the stress-strain curves. Before and after six passes of I-ECAP, the yield strength of the material increases from 308 to 558 MPa and ultimate tensile strength increases from 549 to 685 MPa, this corresponds to 81% and 25% increase respectively. However, after I-ECAP processing, the ductility is somewhat reduced. The uniform elongation (δ_{unif}), which is the elongation of the gauge length just before the on-set of necking, decrease from an initial value of 22.3% to 8.80% after six passes. The elongation to failure (δ_{fail}), also decreases from 31.9% to 20.2%.

It is interesting to note that the uniform elongation (δ_{unif}) achieved in all the processed material condition is significantly lower than the elongation to failure (δ_{fail}). For visual purposes, the uniform elongation (δ_{unif}) is marked by arrows on the individual stress-strain stress curves

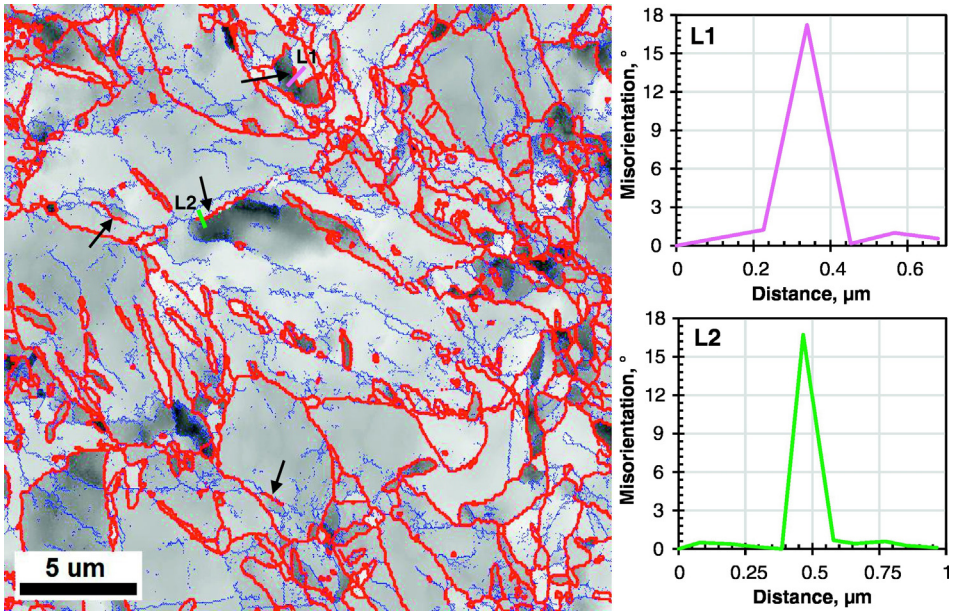

Fig. 14. Higher magnification EBSD map from the second pass sample. Here blue lines represent low angle grain boundaries (LAGBs) between where $2° \le \theta \le 15°$, whereas thick red lines represents the high angle grain boundaries (HAGBs) where $\theta > 15°$. Misorientation profile across two incomplete HAGB segments (L1 and L2) are also shown. (For interpretation of the references to colour in this figure legend, the reader is referred to the web version of this article.)

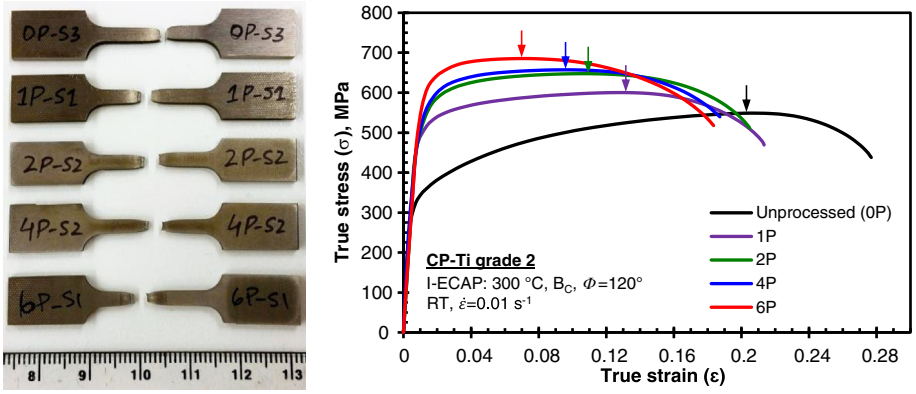

Fig. 15. (a) Fractured flat tensile CP-Ti test specimen from the initial unprocessed condition and after first, second, fourth and sixth pass of I-ECAP and (b) representative plot of true stress-strain curves obtained from tensile testing (the arrows indicate the onset of necking).

in the Fig. 15 (b). Studies [53,54] have shown that, in SPD processed material the onset of necking happens at early stages of deformation during tensile test. This is because SPD processed material contains highly deformed structure, where dislocation density has reached a very high or to some extent a saturation level. Moreover, due to the dynamic recovery process occurring during SPD processing, the grains structure is refined to UFG level, having high and low angle grain boundaries. The UFG material tends to lose the strain hardening behaviour as the very fine grains lose their ability to store dislocations generated during tensile testing, therefore are susceptible to plastic instability (early necking). Hence, in Fig. 15 (b) the processed material exhibits lack of strain hardening behaviour compared to the unprocessed material. Since strain hardening is an important mechanism to sustain uniform elongation (δ_{unif}) during tensile loading, lack of strain hardening exhibited by SPD processed material, limits its ductility. In the present study, however the processed material exhibits increase in post-necking elongation compared to the unprocessed material and therefore it displays acceptable levels of overall ductility (δ_{fail}). It is concluded from the data that, after six passes there is a significant increase in strength without considerable loss of ductility.

4.4.2. Fractography

Fig. 16 (a–e) shows the fracture morphology using SEM of the tensile tested specimens; (a) in the unprocessed condition and after (b) first, (c) second, (d) fourth and (e) sixth pass of I-ECAP. For each material condition, three images are shown; micrograph showing extend of necking at fracture (on the left), lower magnification micrograph (in the middle) and higher magnification micrograph (on the right) of the dotted rectangular box.

Low magnification micrographs (middle figures) of all tested samples confirmed that the fracture surfaces are covered throughout by dimples. This suggests that in all cases, failure process is mainly by nucleation and growth of voids and hence, mode of fracture is entirely ductile in nature. Lower and higher magnification micrographs provided for each sample confirmed that size of the dimples is decreasing with increase in number of passes, which also supports the occurrence of grain refinement process. The unprocessed material is dominated by large size dimples with some evidence of fine size dimples as seen in higher magnification micrograph in Fig. 16 (a). After second pass of I-ECAP process, it is observed that the fraction of large size dimples has been reduced noticeably. After fourth pass, the fractured surface is covered by uniform sized dimples with dimple size reducing even further after sixth pass. Moreover, it is seen that the fracture surface is somewhat smooth after sixth pass.

As listed in Table 3, regardless of the number of passes the reduced area at failure (Ψ) is somewhat similar, having values between 60.1 and 59.5%. As discussed earlier, although the onset of necking in processed material happens at early stages of deformation, the area at failure (Ψ) values suggest resistance to localized necking. This can be considered as a possible explanation for area at failure (Ψ) having similar values.

Table 3
Tensile properties of CP-Ti in unprocessed condition and after subsequent I-ECAP passes (0.2% σ_Y — yield strength, σ_{UTS} — ultimate tensile strength, δ_{unif} — uniform elongation, δ_{fail} — elongation to failure, Ψ — reduced cross-section area at failure, ε_{fail} — true strain at failure and σ_{fail} — true stress at failure).

Pass #	Equivalent strain	0.2% σ_Y (MPa)	σ_{UTS} (MPa)	δ_{unif} (%)	δ_{fail} (%)	Ψ (%)	ε_{fail}	σ_{fail} (MPa)
0P	–	308	549	22.3	31.9	63.9	0.28	438
1P	0.67	489	601	14.5	23.8	60.1	0.21	469
2P	1.34	502	648	12.7	22.8	59.6	0.20	511
4P	2.68	511	657	11.4	20.6	60.2	0.18	539
6P	4.02	558	685	8.8	20.2	59.5	0.18	517

4.4.3. Compression testing

Fig. 17 represents true stress as a function of true strain determined by uniaxial compression testing conducted at room temperature for (a) unprocessed and (b) severely deformed CP-Ti after six passes of I-ECAP, respectively. To investigate any strain rate sensitivity at room temperature, tests were performed at three different strain rates ($\dot{\varepsilon}$): 0.01, 0.10 and 1.00 s^{-1}. All tests were conducted up to 50% height reduction, resulting in a true strain value of ~0.70.

First, it is apparent from the obtained flow curves that the processed material shows significant increase in compressive yield strength for all strain rates compared to unprocessed material. This shows again that the material has strengthen due to grain refinement process. However, the test results shows that the severely deformed material displays lower levels of strain hardening compared to unprocessed material. It is interesting to note, that although the yield strength of the processed material is higher, the unprocessed material due its greater strain hardening ability quickly strengthens during compression and displays a higher flow stress beyond the ~0.30 true strain value. For all strain rates, the unprocessed material therefore manages to achieve higher flow stress values at completion of compression tests at ~0.70 true strain.

In order to study the strain hardening behaviour in detail during these compression tests, Fig. 18 presents plot of normalized strain hardening rate ($d\sigma/d\varepsilon/G$) against true strain for (a) unprocessed material and (b) processed material. Where σ is the flow stress, ε is the true strain and G is the shear modulus (modulus of rigidity) for titanium. In general, both material condition exhibits a distinct three-stage strain hardening behaviour within the plastic regime. Stage I is characterized

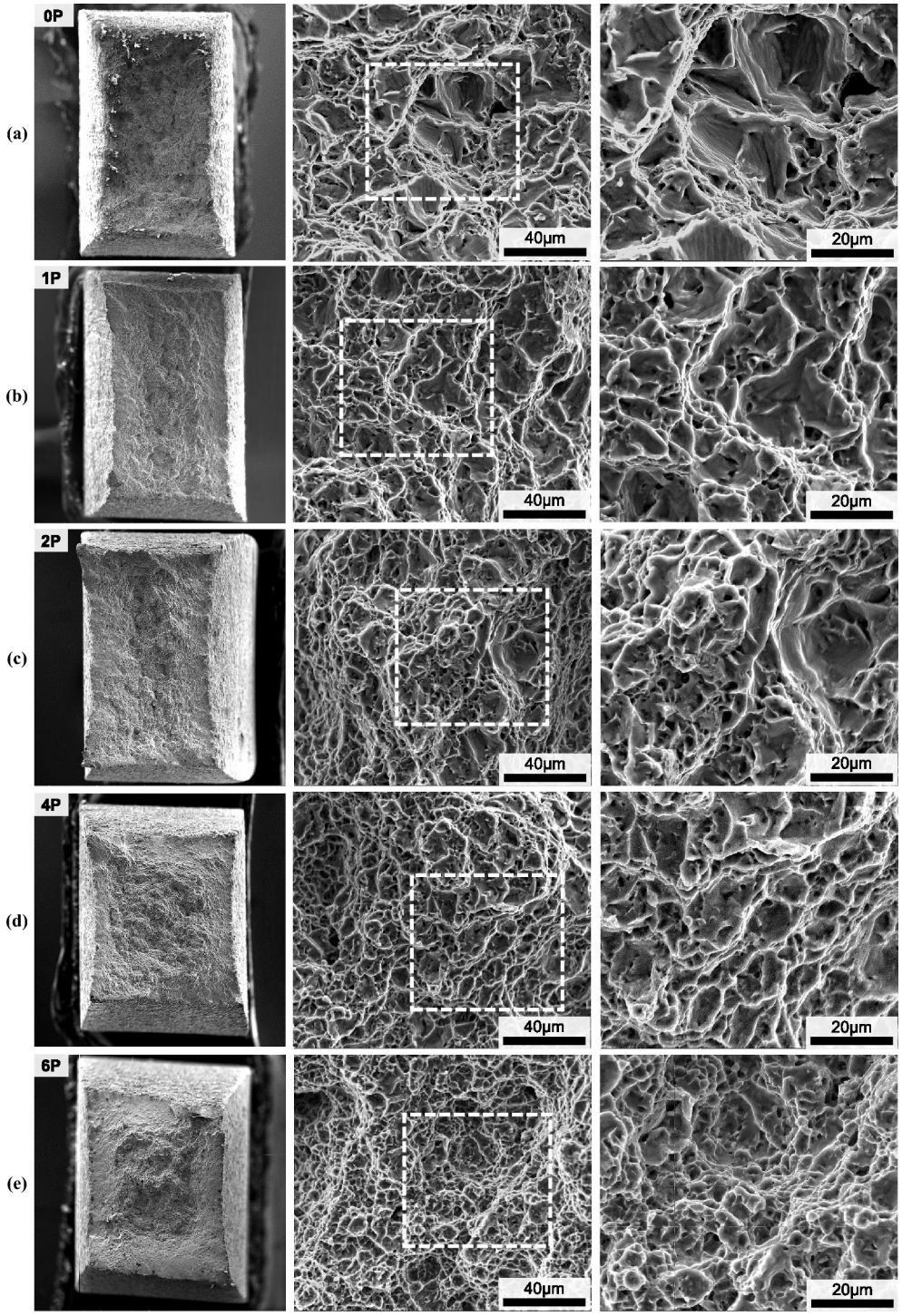

Fig. 16. Scanning electron microscope (SEM) images of the fractured tensile samples showing the fracture morphology for unprocessed and I-ECAP processed samples.

by a decreasing rate of strain hardening and is similar to the dynamic recovery regime observed in many metals [55]. Upon reaching a certain strain, the hardening rate increases, representing the stage II deformation. This is then followed by considerable reduced rate of hardening or even flow softening (negative rate of hardening), denoting the stage III deformation. This three-stage hardening behaviour is consistent with earlier reports on compression testing of titanium at room and elevated temperatures [55–57].

Studies have shown that the increase in strain hardening behaviour in stage II is due to deformation twinning [58,59]. Notice that the severely deformed CP-Ti in Fig. 18 (b), exhibits much lower levels of stage II strain hardening compared to the unprocessed material. This is because the severely deformed material has a UFG structure; therefore, twinning activity is greatly suppressed as such. The results are consistent with Gray [60], who performed compression tests on fine and coarse grain titanium, which shows that the rate of strain hardening increases with increase in grain size due to pronounced increase in deformation twinning. Twinning increases the strain hardening in two ways; firstly, it causes reduction in effective grain size, therefore contributes to strengthening via the Hall-Patch effect. Secondly, the twinned regions are much harder than the rest of the matrix (untwinned) regions. To confirm the later, Kalidindi et al. [58] deformed CP-Ti under

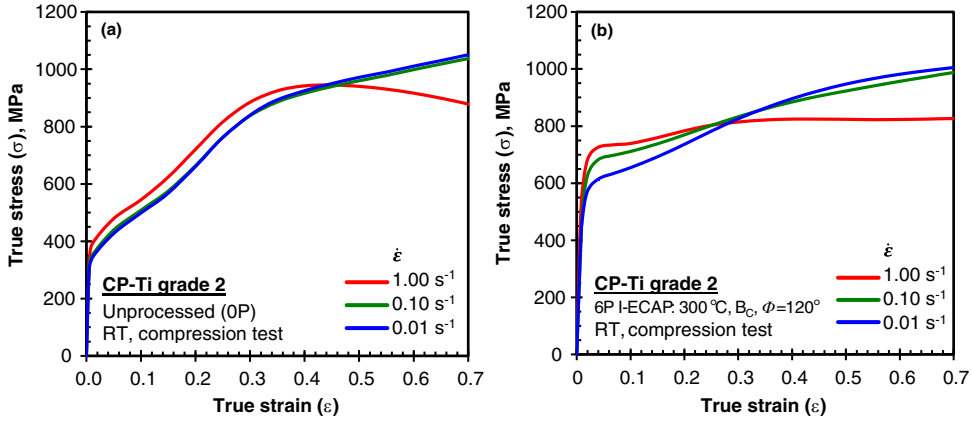

Fig. 17. Representative flow curves (true stress vs true strain) obtained from uniaxial compression testing at various strain rates for (a) unprocessed material and (b) after six passes of I-ECAP.

compression up to a strain of 5%, this corresponds to the initiation of stage II hardening and onset of deformation twinning. Microhardness measurement on the twinned regions showed a 30% hardness increase compared to the matrix regions.

Notice that the onset of stage II strain hardening in the present study also happens around ~5% true strain (see Fig. 18 (a) and (b)). However in Fig. 18 (a) it is seen that the initiation of stage II hardening for the fastest strain rate of 1.0 s^{-1} (red line) happens slightly earlier i.e. at a lower true strain value compared to the slower strain rates (green and blue lines). Similar results were obtained in [61], in which it was shown that deformation twins are generated at lower strains during compression as the strain rate is increased. However, this effect is not observed in the severely deformed material, where the onset of stage II hardening does not seems to be effected by the increase in strain rate.

For strain rates of 0.01 and 0.1 s^{-1}, the unprocessed material during stage III shows a rapidly decreasing strain hardening behaviour. However, beyond a true strain of ~0.40 both reaches a steady state condition and there is no noticeable change in strain hardening rate. For the severely deformed material at these strain rates, the decrease in strain hardening in stage III is not as rapid. It decreases at a lower rate and continues to do so until test finishes.

Compression tests have shown that, the severely deformed material has still some tendency of strain hardening compared to tensile tests, where a near steady state behaviour in flow stress was observed after initial yielding. Nevertheless, both the tensile and compression tests results have shown that the processed material significantly loses its ability to strain harden compared to unprocessed material. This is because the heavily deformed UFG structure in the processed material has a limited capacity to accumulate further dislocations and has a reduced tendency to generate twin boundaries during subsequent deformation [62].

For both material condition the flow stress obtained at the highest strain rate of 1.0 s^{-1} is particularly interesting, after an initial strain hardening behaviour (stage I and stage II), both exhibited flow softening (negative rate of hardening). However, this flow softening is much more prominent in unprocessed material. The observed flow softening is believed due to the temperature rise during deformation. This flow softening at a strain rate of 1.0 s^{-1}, has also been observed during compression tests on nanocrystalline titanium produced by mechanical milling followed by a consolidation process [63] and also in UFG titanium produced by ECAP [64]. Both studies concluded, the flow softening due to the heat generated during plastic deformation. The temperature rise during deformation can be calculated by the following relationship:

$$\Delta T = \frac{\beta}{\rho C_p}\int_0^{\varepsilon}\sigma \cdot d\varepsilon \tag{2}$$

where β is the factor which specifies the portion of plastic work converted into heat (Taylor-Quinney coefficient, normally taken to be 0.90), ρ is the material's density, C_p is the specific heat and the integral in Eq. (2) defines the work done by flow stress (σ) during compression loading. Using the equation, the temperature rise during compression testing is calculated for two strain levels: (1) true strain where flow softening begins (ε_s) and (2) the final true strain ($\varepsilon_f \approx 0.70$). Ideal conditions are

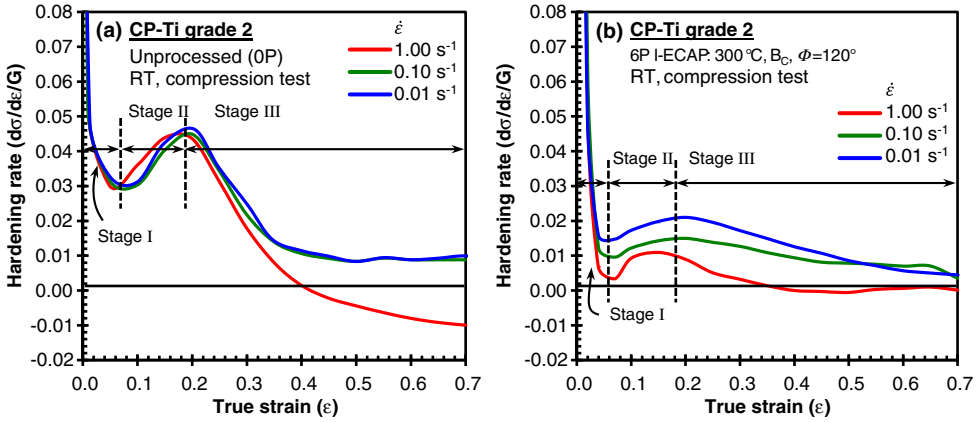

Fig. 18. Plot of normalized strain hardening behaviour for (a) unprocessed and (b) severely deformed material after six passes. (For interpretation of the references to color in this figure, the reader is referred to the web version of this article.)

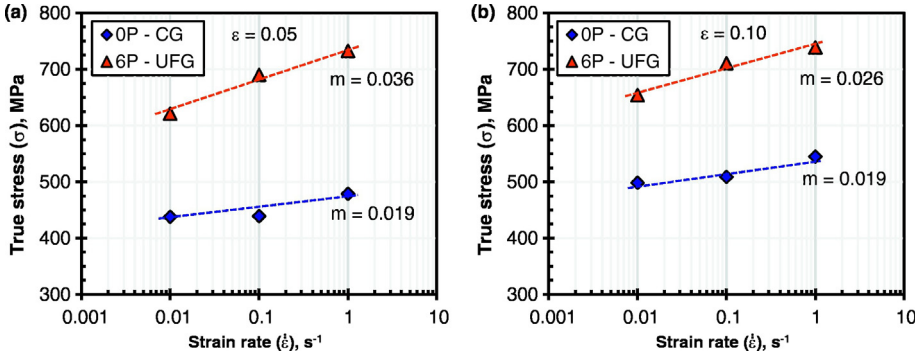

Fig. 19. Strain rate sensitivity at room temperature of (a) unprocessed (0P-CG) material and (b) material (6P-UFG) after six passes of I-ECAP.

assumed, i.e. no heat loss due to conduction or convection. For unprocessed material the equation predicts a temperature rise of 121 °C at $\varepsilon_s = 0.45$ which increases to 219 °C at ε_f. The predicted temperature rise for processed material is 81 °C at $\varepsilon_s = 0.28$ and rises to 198 °C at ε_f. The flow stress of titanium is very sensitive to temperature, the predicted temperature rise at strain rate of 1.0 s^{-1} for both material conditions is assumed to influence the flow stress behaviour. However, further tests such as load-unload-reload tests performed in [63] are necessary to establish the exact role of temperature rise in flow softening.

The flow stress of severely deformed material displays higher level of dependence on strain rate, whereby the flow stress increases with increase in strain rate. The unprocessed material only shows increase in flow stress at the highest strain rate of 1.0 s^{-1}. The effect of strain rate on the flow stress of the material can be further analysed by determining the strain rate sensitivity. The strain rate sensitivity is denoted by m value and is calculated by Eq. (3):

$$m = \left.\frac{\partial \log\sigma}{\partial \log\dot{\varepsilon}}\right|_{\varepsilon,T} \tag{3}$$

where σ and $\dot{\varepsilon}$ are the flow stress and strain rate, respectively. It is important to note that the m value has to be calculated for a certain strain value and temperature. Fig. 19 (a) and (b) shows the variation of flow stress on various strain rates plotted on a semi-logarithmic form, where stress is measured at (a) 5% and (b) 10% true strain, respectively for coarse grain (0P) and UFG (6P) material tested in compression at room temperature. The values of strain rate sensitivity can be easily calculated from such graph, by determining the slope of the linear fit.

It is apparent that the m value at both selected strains shown in Fig. 19 for the UFG material is higher compared to unprocessed material. From the flow stress observation and the m value calculation, it is shown that the UFG Ti exhibits a higher strain rate sensitivity in compression at room temperature. Although the UFG material exhibits increase strain rate sensitivity, this increase is not believed to improve the ductility of the material considerably during tensile deformations at room temperature. This is because the mechanisms such as grain boundary sliding which facilitates increase in ductility occurring in higher strain rate sensitive materials are not pronounced at room temperature [65].

4.5. Hardness evolution

Numerous studies on ECAP have shown that it is essential to process the billet multiple times in order to induce the desired level of strain and thereby attain UFG structure. Microhardness is considered as a standard procedure for evaluating the induced strain after processing and also to study the level of billet homogeneity with respect to mechanical properties and corresponding microstructural changes. To examine the homogeneity of strain distribution and also to investigate the evolution of hardness with increasing number of I-ECAP passes, microhardness measurements were recorded both on unprocessed material and on material subjected to I-ECAP passes. The individual values of microhardness (Hv) were measured on an 11 × 11 array of equi-spaced points across the transverse (X) plane.

For the purposes of providing a detailed visual representation, contour maps have been generated from the microhardness measurements across the X plane. The Fig. 20 (a–e) shows colour-coded contour maps for the (a) unprocessed material and for the (b) first, (c) second, (d) fourth and (e) sixth pass. For all maps, the values of microhardness are represented by a set of distinct colours. The corresponding microhardness value of each colour is shown by the legend given on the right, which ranges from 150 to 220 Hv in increments of 7 Hv. The X and Y axis of the plot represent the transverse direction (TD) and normal direction (ND) with flow direction (FD) pointing outward from the paper.

It is evident from Fig. 20 (b), that the microhardness values increases significantly after the first pass and this increase is seen to occur over the entire surface of the sample. The increase in microhardness continues through subsequent passes, this is attributed to the fact that greater level of strain is accumulated in the material after each pass which causes reduction in grain size thereby increasing the strength characteristic of the material. However, upon close assessment of the contour plot, it is evident that the increase in the hardness distribution is not completely uniform across the entire surface. There is a region of lower hardness near the top surface of the billet after fourth pass. Although, after sixth pass the situation improves, as this region of lower hardness is somewhat shrinked. Nevertheless, this narrow region of lower hardness near the top remains even after six passes.

In order to examine the level of non-uniformity, Fig. 21 (a–d) shows the microhardness (Hv) values recorded on the transverse (X) plane along the centre line and at 1 mm from the top and bottom surfaces after (a) one, (b) two, (c) four and (d) six passes respectively. For all the plots the dashed line represents the average microhardness in the unprocessed condition. Overall, it is fairly obvious that the microhardness values are increasing with increasing number of passes. After first pass, the average microhardness along the centre line increases to ~180 Hv from ~157 Hv in the unprocessed condition. The microhardness values near the top surface was lower with a value of ~175 Hv, however near the bottom surface the average value was slightly higher with ~182 Hv. From pass two to six the hardness continues to increase gradually over subsequent passes and does not seems to saturate. The level of homogeneity improves after second pass since the microhardness near the top and bottom surfaces are relatively similar to microhardness along the centre line. Beyond pass two, the region near the bottom surface continues to maintain the same hardness level as the centre line. In contrast, the hardness near the top surface is somewhat lower. After six passes, average microhardness at the centre line and near the bottom surface are both roughly the same at ~218 Hv, compared to a value of ~210 Hv near the top surface.

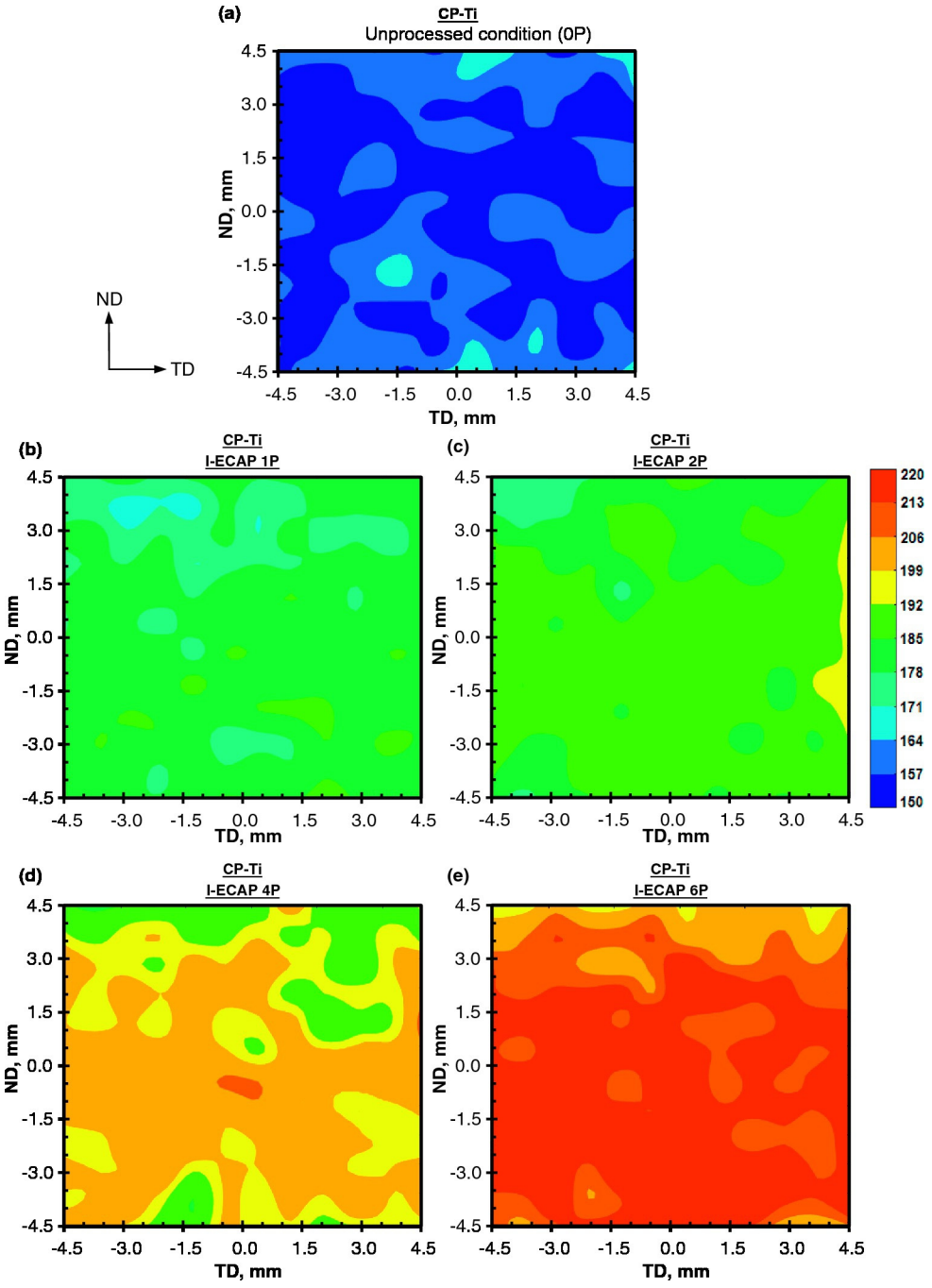

Fig. 20. Colour coded contour maps of the microhardness (*Hv*) values recorded on the transverse (X) plane of (a) unprocessed condition, after (b) first, (c) second, (d) fourth and (e) sixth pass of the I-ECAP process. (For interpretation of the references to color in this figure, the reader is referred to the web version of this article.)

Fig. 22 shows the mean values of microhardness calculated from the recorded measurements on the X plane of samples, for unprocessed condition and after first, second, fourth and sixth passes of I-ECAP. The error bars in the graph represent the standard deviation, which shows the level of dispersion in the hardness values from the mean value. In the unprocessed condition the mean value of microhardness is ~156 *Hv*, after first pass this value rises sharply to ~181 *Hv*, an increase of 16%. For subsequent second, fourth and sixth passes the microhardness value increases to 187, 199 and 215 *Hv*, this corresponds to an increase of 3.3%, 6.4% and 8.0% respectively. This increase in mean microhardness values also correlates qualitatively with the increase in yield and ultimate tensile strength observed in tensile test after subsequent I-ECAP passes. Overall, after six passes of I-ECAP process the average value of microhardness is increased from 156 to 215 *Hv*, this corresponds to an increase of 38%.

5. Comparison with ECAP

It is convenient to make a comparison with the earlier reports of processing CP-Ti (various grades) by ECAP at different die angles, processing speeds and temperatures. Table 4 presents the summary of processing parameters used in selected earlier ECAP studies and present study, along with the improvement in grain size, hardness, strength and ductility. It is important to emphasize that the grain size and mechanical properties listed in the table are after ECAP process only and before any subsequent post ECAP deformation (such as cold extrusion, rolling etc.)

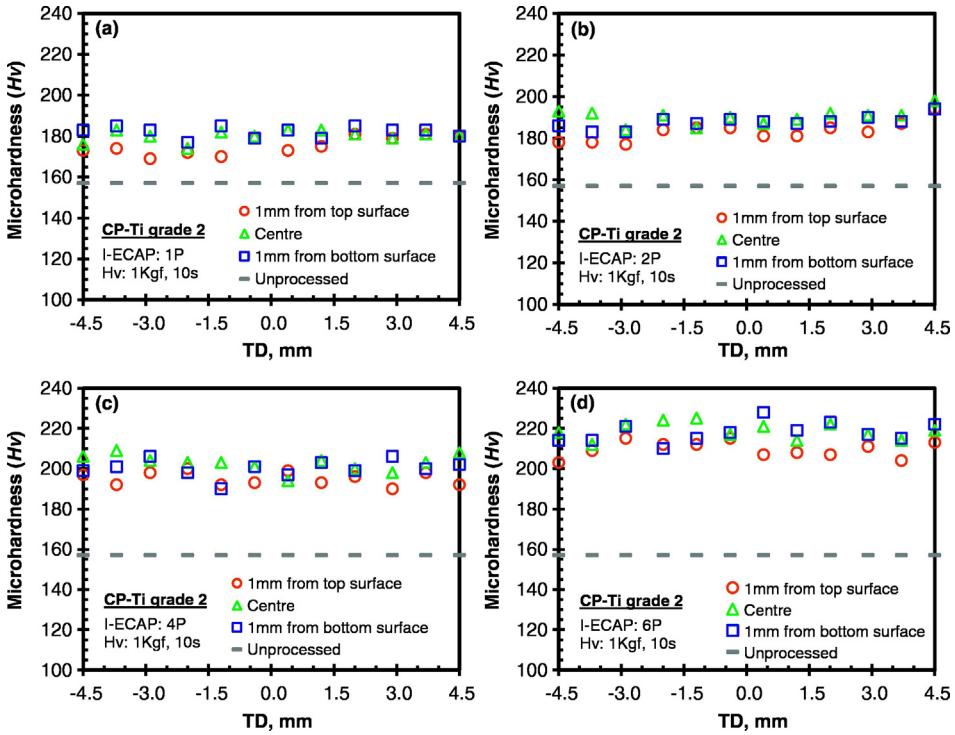

Fig. 21. Microhardness (*Hv*) values recorded on the transverse (X) plane along the centre and at 1 mm from the top and bottom surfaces after (a) first, (b) second, (c) fourth and (d) sixth pass of the I-ECAP process: the dashed line shows the average microhardness value in the unprocessed condition.

are performed. The table has been arranged in the descending order of processing temperature.

As can be seen in the table, to facilitate processing of CP-Ti various techniques have been employed. These include processing at elevated temperatures, using higher die angles and by using lower grades of titanium. To activate more slip systems in titanium, almost all the studies listed in table have been performed at elevated temperatures (500 to 250 °C). Zhao et al. [30,31] was however able to demonstrate ECAP at room temperature. This is because grade 1 was used in these studies, which has the lowest interstitial and substitutional elements among available commercial grades of titanium and therefore considered to be the most formable.

In the context of processing grade 2; for lower die angle of 90°, the processing temperature was 350 °C or above. However, it is seen that the processing temperature can be decreased to 250 °C, when higher die angles of 105 to 120° is used. It is evident from the table that the enhancements in mechanical properties by I-ECAP achieved in the present study are quite reasonably comparable with previous ECAP studies. Although, lowering the processing temperature or by using 90° die, the enhancements in mechanical properties can be improved even further.

The study by Sordi et al. [72] is directly comparable with the present study, as it has identical processing conditions. It is seen that although the processing conditions are exactly the same, the mechanical properties are better to the ones obtained in the present study. However upon analysing the Fig. 5 in [72] whereby the tensile flow stress curves are presented. It is clear that the material after subsequent ECAP passes, suffers a very high rate of flow softening beyond the onset of necking, which is not the case in the present study. Moreover, the uniform elongation is also considerably less than the one observed in the present study.

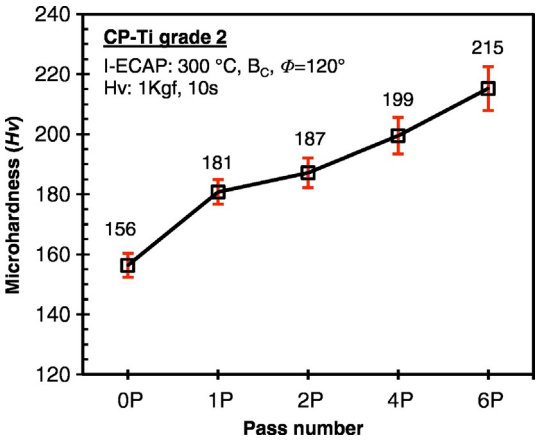

Fig. 22. Mean values of Vickers microhardness (*Hv*) recorded on the X plane before and after subsequent passes of I-ECAP process.

6. Conclusion

The feasibility of using the I-ECAP process for refining grain structure in CP-Ti with the objective of improving its strength characteristics has been presented in this article. CP-Ti grade 2 billets were successfully processed via double-billet variant of I-ECAP process. The billets were subjected to a total of six passes at 300 °C following route B_C, using the die channel intersection angle of 120°. The following conclusions are drawn from the results obtained:

1. I-ECAP process is shown to be an effective method which is capable of producing defect free CP-Ti billets. This promising technique requires very low pressing force therefore it is capable of processing very long or continuous billets.
2. Initial passes of I-ECAP process resulted in a heterogeneous microstructure. EBSD analysis of subsequent passes reveals remarkable grain refinement leading to homogenous UFG microstructure. The average grain size of the as received material was reduced from ~22 μm to ~0.89 μm after sixth pass. The texture analysis showed that a fibre texture formed immediately after first pass. Its strength continues to increase up to fourth pass, after which it weakens due to significant grain refinement.

Table 4
Summary of CP-Ti processing parameters used in selected earlier ECAP studies and present study, along with the improvement in grain size, hardness, strength and ductility.

Reference	Ti grade	Die angle	Speed mm/s	Temp °C	Route	N	Grain size μm	*Hv*	σ_y MPa	σ_{UTS} MPa	δ_{fail} %
Stolyarov et al. [66]	3	90°	–	450–500	B_C	7	0.30	240	520	540	16
Stolyarov et al. [40]	3	90°	6.0	400–450	B_A, B_C, C	8	0.26–0.47	266–277	640–720	710–760	10–4
Latysh et al. [67]	2	90°	–	450	–	4	0.30–0.70	–	545	630	22
Chen et al. [52]	2	90°		450	A	4					
Kang and Kim [68]	2	90°	2.0	450	A-C-C-A	5	0.96		530	665	26.0
Hyun and Kim [69]	2	110°	–	410	B_C	6	0.30	–	580	740	19.6
Rao et al. [70]	1	120°	6	400	B_C	3	–	180	423	463	30.0
Ko et al. [23]	2	90°	0.10	350	C	8	0.30	–	655	–	13
Bindu et al. [71]	2	90°	–	350	B_C	4	0.24	–	418	–	–
This study	2	120°	0.10	300	B_C	6	0.89	215	558	685	20.2
Sordi et al. [72]	2	120°	0.08	300	B_C	6	–	248	615	790	32.0
Purcek et al. [73]	2	90°	1.27	300	E	8	0.30		620	760	21.0
Medvedev et al. [24]	2	90°	1	300	B_C	4	0.20	–	750	850	18.0
Hajizadeh et al. [22]	2	105°	1	250	–	10	0.21	280	750	892	20.5
Zhao et al. [30]	1	120°	2.0	RT	B_C	8	0.20		710	790	19.0
Zhao et al. [31]	1	90°	3.5	RT	C	4	0.15	236	–	765	48.0

3. Careful analysis of the second pass sample revealed incomplete HAGB segments with misorientation angle slightly above 15°. This is as a strong evidence for the occurrence of continuous dynamic recrystallization (CDRX) phenomena.
4. Severely deformed material exhibited significant improvement in the mechanical properties. During room temperature tensile testing, the yield strength of the material increased from 308 to 558 MPa and ultimate tensile strength increased from 548 to 685 MPa. This corresponds to 81% and 25% increase, respectively. However, the ductility was somewhat reduced due to lack of strain hardening ability exhibited by severely deformed material.
5. Compression tests at various strain rates before and after I-ECAP processing revealed a distinct three-stage strain hardening behaviour. However, the UFG CP-Ti due to its reduced tendency to generate deformation twins, showed a much lower strain hardening rate during stage II hardening. The severely deformed material displayed enhancement in compressive yield strength, as well as higher strain rate sensitivity compared to the unprocessed material.
6. The evolution of hardness during subsequent passes of I-ECAP was investigated by recording Vickers microhardness measurements along the transverse plane. Hardness homogeneity was fairly uniform except for the narrow region at the top. Average value of microhardness was significantly increased from 156 to 215 *Hv*, an increase of 38%.

Acknowledgement

This work has been partially funded by the EPSRC SAMULET Project 4 with grant number EP/G03477X/1.

Appendix A. Supplementary data

Supplementary data to this article can be found online at http://dx.doi.org/10.1016/j.matdes.2017.03.015.

References

[1] D.M. Brunette, P. Tengvall, M. Textor, P. Thomsen, Titanium in Medicine: Material Science, Surface Science, Engineering, Biological Responses and Medical Applications, Springer-Verlag, Berlin Heidelberg New York, 2001.
[2] M. Geetha, A.K. Singh, R. Asokamani, A.K. Gogia, Ti based biomaterials, the ultimate choice for orthopaedic implants – a review, Prog. Mater. Sci. 54 (3) (2009) 397–425.
[3] K. Alvarez, H. Nakajima, Metallic scaffolds for bone regeneration, Materials 2 (3) (2009) 790.
[4] S.J. Lugowski, D.C. Smith, A.D. McHugh, J.C. Van Loon, Release of metal ions from dental implant materials in vivo: determination of Al, Co, Cr, Mo, Ni, V, and Ti in organ tissue, J. Biomed. Mater. Res. 25 (12) (1991) 1443–1458.
[5] M.A. Meyers, A. Mishra, D.J. Benson, Mechanical properties of nanocrystalline materials, Prog. Mater. Sci. 51 (4) (2006) 427–556.
[6] T.G. Langdon, Twenty-five years of ultrafine-grained materials: achieving exceptional properties through grain refinement, Acta Mater. 61 (19) (2013) 7035–7059.
[7] A. Balyanov, J. Kutnyakova, N.A. Amirkhanova, V.V. Stolyarov, R.Z. Valiev, X.Z. Liao, Y.H. Zhao, Y.B. Jiang, H.F. Xu, T.C. Lowe, Y.T. Zhu, Corrosion resistance of ultra fine-grained Ti, Scr. Mater. 51 (3) (2004) 225–229.
[8] I.P. Semenova, G.K. Salimgareeva, V.V. Latysh, T. Lowe, R.Z. Valiev, Enhanced fatigue strength of commercially pure Ti processed by severe plastic deformation, Mater. Sci. Eng. A 503 (1–2) (2009) 92–95.
[9] Y. Estrin, A. Vinogradov, Extreme grain refinement by severe plastic deformation: a wealth of challenging science, Acta Mater. 61 (3) (2013) 782–817.
[10] R.Z. Valiev, R.K. Islamgaliev, I.V. Alexandrov, Bulk nanostructured materials from severe plastic deformation, Prog. Mater. Sci. 45 (2) (2000) 103–189.
[11] R.Z. Valiev, T.G. Langdon, Principles of equal-channel angular pressing as a processing tool for grain refinement, Prog. Mater. Sci. 51 (7) (2006) 881–981.
[12] T.G. Langdon, The principles of grain refinement in equal-channel angular pressing, Mater. Sci. Eng. A 462 (1–2) (2007) 3–11.
[13] A.P. Zhilyaev, T.G. Langdon, Using high-pressure torsion for metal processing: fundamentals and applications, Prog. Mater. Sci. 53 (6) (2008) 893–979.
[14] Y. Saito, H. Utsunomiya, N. Tsuji, T. Sakai, Novel ultra-high straining process for bulk materials—development of the accumulative roll-bonding (ARB) process, Acta Mater. 47 (2) (1999) 579–583.
[15] V.M. Segal, S.V. Dobatkin, R.Z. Valiev, Equal-channel angular pressing of metallic materials: achievements and trends. Selection of articles: part I, Russ. Metall. 1 (2004) 1–102.
[16] V.M. Segal, V.I. Reznikov, A.E. Drobyshevskiy, V.I. Kopylov, Plastic metal working by simple shear, Russ. Metall. 1 (1981) 99–104.
[17] Y. Iwahashi, Z. Horita, M. Nemoto, T.G. Langdon, The process of grain refinement in equal-channel angular pressing, Acta Mater. 46 (9) (1998) 3317–3331.
[18] Y. Iwahashi, M. Furukawa, Z. Horita, M. Nemoto, T.G. Langdon, Microstructural characteristics of ultrafine-grained aluminum produced using equal-channel angular pressing, Metall. Mater. Trans. A 29 (9) (1998) 2245–2252.
[19] M. Furukawa, Y. Iwahashi, Z. Horita, M. Nemoto, T.G. Langdon, The shearing characteristics associated with equal-channel angular pressing, Mater. Sci. Eng. A 257 (2) (1998) 328–332.
[20] M. Furukawa, Z. Horita, T.G. Langdon, Factors influencing the shearing patterns in equal-channel angular pressing, Mater. Sci. Eng. A 332 (1–2) (2002) 97–109.
[21] S.L. Semiatin, D.P. DeLo, Equal channel angular extrusion of difficult-to-work alloys, Mater. Des. 21 (4) (2000) 311–322.
[22] K. Hajizadeh, B. Eghbali, K. Topolski, K.J. Kurzydlowski, Ultra-fine grained bulk CP-Ti processed by multi-pass ECAP at warm deformation region, Mater. Chem. Phys. 143 (3) (2014) 1032–1038.
[23] Y.G. Ko, D.H. Shin, K.-T. Park, C.S. Lee, An analysis of the strain hardening behavior of ultra-fine grain pure titanium, Scr. Mater. 54 (10) (2006) 1785–1789.
[24] A. Medvedev, H.P. Ng, R. Lapovok, Y. Estrin, T.C. Lowe, V.N. Anumalasetty, Comparison of laboratory-scale and industrial-scale equal channel angular pressing of commercial purity titanium, Mater. Lett. 145 (0) (2015) 308–311.
[25] P. Rodriguez-Calvillo, J.M. Cabrera, Microstructure and mechanical properties of a commercially pure Ti processed by warm equal channel angular pressing, Mater. Sci. Eng. A 625 (0) (2015) 311–320.
[26] A.V. Sergueeva, V.V. Stolyarov, R.Z. Valiev, A.K. Mukherjee, Advanced mechanical properties of pure titanium with ultrafine grained structure, Scr. Mater. 45 (7) (2001) 747–752.
[27] Y. Zhang, R.B. Figueiredo, S.N. Alhajeri, J.T. Wang, N. Gao, T.G. Langdon, Structure and mechanical properties of commercial purity titanium processed by ECAP at room temperature, Mater. Sci. Eng. A 528 (25–26) (2011) 7708–7714.

[28] V.V. Stolyarov, Y.T. Zhu, T.C. Lowe, R.Z. Valiev, Microstructure and properties of pure Ti processed by ECAP and cold extrusion, Mater. Sci. Eng. A 303 (1–2) (2001) 82–89.
[29] V.V. Stolyarov, L. Zeipper, B. Mingler, M. Zehetbauer, Influence of post-deformation on CP-Ti processed by equal channel angular pressing, Mater. Sci. Eng. A 476 (1–2) (2008) 98–105.
[30] X. Zhao, X. Yang, X. Liu, X. Wang, T.G. Langdon, The processing of pure titanium through multiple passes of ECAP at room temperature, Mater. Sci. Eng. A 527 (23) (2010) 6335–6339.
[31] X. Zhao, X. Yang, X. Liu, C.T. Wang, Y. Huang, T.G. Langdon, Processing of commercial purity titanium by ECAP using a 90 degrees die at room temperature, Mater. Sci. Eng. A 607 (0) (2014) 482–489.
[32] G.J. Raab, R.Z. Valiev, T.C. Lowe, Y.T. Zhu, Continuous processing of ultrafine grained Al by ECAP–Conform, Mater. Sci. Eng. A 382 (1–2) (2004) 30–34.
[33] J.-C. Lee, H.-K. Seok, J.-H. Han, Y.-H. Chung, Controlling the textures of the metal strips via the continuous confined strip shearing(C2S2) process, Mater. Res. Bull. 36 (5–6) (2001) 997–1004.
[34] Y. Saito, H. Utsunomiya, H. Suzuki, T. Sakai, Improvement in the r-value of aluminum strip by a continuous shear deformation process, Scr. Mater. 42 (12) (2000) 1139–1144.
[35] Y. Huang, P.B. Prangnell, Continuous frictional angular extrusion and its application in the production of ultrafine-grained sheet metals, Scr. Mater. 56 (5) (2007) 333–336.
[36] A. Rosochowski, L. Olejnik, FEM simulation of incremental shear, AIP Conf. Proc. 907 (1) (2007) 653–658.
[37] A. Rosochowski, L. Olejnik, M.W. Richert, Double-billet Incremental ECAP, Mater. Sci. Forum, Trans Tech Publ, 2008 139–144.
[38] L. Olejnik, A. Rosochowski, M.W. Richert, Incremental ECAP of Plates, Mater. Sci. Forum, Trans Tech Publ, 2008 108–113.
[39] A. Rosochowski, M. Rosochowska, L. Olejnik, B. Verlinden, Incremental equal channel angular pressing of sheets, Proc. 13th International Conference on Metal Forming, Japan 2010, Steel Research International 2010, pp. 470–473.
[40] V.V. Stolyarov, Y.T. Zhu, I.V. Alexandrov, T.C. Lowe, R.Z. Valiev, Influence of ECAP routes on the microstructure and properties of pure Ti, Mater. Sci. Eng. A 299 (1–2) (2001) 59–67.
[41] N.P. Gurao, G. Manivasagam, P. Govindaraj, R. Asokamani, S. Suwas, Effect of texture and grain size on bio-corrosion response of ultrafine-grained titanium, Metall. Mater. Trans. A 44 (12) (2013) 5602–5610.
[42] V.M. Segal, Engineering and commercialization of equal channel angular extrusion (ECAE), Mater. Sci. Eng. A 386 (1–2) (2004) 269–276.
[43] I.H. Son, Y.G. Jin, Y.T. Im, S.H. Chon, J.K. Park, Sensitivity of friction condition in finite element investigations of equal channel angular extrusion, Mater. Sci. Eng. A 445–446 (2007) 676–685.
[44] Y.T. Zhu, T.C. Lowe, Observations and issues on mechanisms of grain refinement during ECAP process, Mater. Sci. Eng. A 291 (1–2) (2000) 46–53.
[45] I. Kim, J. Kim, D.H. Shin, C.S. Lee, S.K. Hwang, Effects of equal channel angular pressing temperature on deformation structures of pure Ti, Mater. Sci. Eng. A 342 (1–2) (2003) 302–310.
[46] D.H. Shin, I. Kim, J. Kim, Y.S. Kim, S.L. Semiatin, Microstructure development during equal-channel angular pressing of titanium, Acta Mater. 51 (4) (2003) 983–996.
[47] Y.J. Chen, Y.J. Li, J.C. Walmsley, S. Dumoulin, S.S. Gireesh, S. Armada, P.C. Skaret, H.J. Roven, Quantitative analysis of grain refinement in titanium during equal channel angular pressing, Scr. Mater. 64 (9) (2011) 904–907.
[48] A. Ghaderi, M.R. Barnett, Sensitivity of deformation twinning to grain size in titanium and magnesium, Acta Mater. 59 (20) (2011) 7824–7839.
[49] C.S. Meredith, A.S. Khan, The microstructural evolution and thermo-mechanical behavior of UFG Ti processed via equal channel angular pressing, J. Mater. Process. Technol. 219 (0) (2015) 257–270.
[50] Y.J. Chen, Y.J. Li, J.C. Walmsley, S. Dumoulin, H.J. Roven, Deformation structures of pure titanium during shear deformation, Metall. Mater. Trans. A 41 (4) (2010) 787–794.
[51] F.J. Humphreys, M. Hatherly, Recrystallization and Related Annealing Phenomena, second ed. Elsevier, Oxford, 2004.
[52] Y.J. Chen, Y.J. Li, J.C. Walmsley, S. Dumoulin, P.C. Skaret, H.J. Roven, Microstructure evolution of commercial pure titanium during equal channel angular pressing, Mater. Sci. Eng. A 527 (3) (2010) 789–796.
[53] Y.M. Wang, E. Ma, Three strategies to achieve uniform tensile deformation in a nanostructured metal, Acta Mater. 52 (6) (2004) 1699–1709.
[54] Y. Wang, M. Chen, F. Zhou, E. Ma, High tensile ductility in a nanostructured metal, Nature 419 (6910) (2002) 912–915.
[55] A.A. Salem, S.R. Kalidindi, R.D. Doherty, Strain hardening regimes and microstructure evolution during large strain compression of high purity titanium, Scr. Mater. 46 (6) (2002) 419–423.
[56] S. Nemat-Nasser, W.G. Guo, J.Y. Cheng, Mechanical properties and deformation mechanisms of a commercially pure titanium, Acta Mater. 47 (13) (1999) 3705–3720.
[57] Z. Zeng, Y. Zhang, S. Jonsson, Deformation behaviour of commercially pure titanium during simple hot compression, Mater. Des. 30 (8) (2009) 3105–3111.
[58] S.R. Kalidindi, A.A. Salem, R.D. Doherty, Role of deformation twinning on strain hardening in cubic and hexagonal polycrystalline metals, Adv. Eng. Mater. 5 (4) (2003) 229–232.
[59] A.A. Salem, S.R. Kalidindi, R.D. Doherty, Strain hardening of titanium: role of deformation twinning, Acta Mater. 51 (14) (2003) 4225–4237.
[60] G.T. Gray, Influence of strain rate and temperature on the structure. Property behavior of high-purity titanium, J. Phys. IV 07 (C3) (1997) 423–428.
[61] K. Ahn, H. Huh, J. Yoon, Rate-dependent hardening model for pure titanium considering the effect of deformation twinning, Int. J. Mech. Sci. 98 (2015) 80–92.
[62] D. Jia, Y.M. Wang, K.T. Ramesh, E. Ma, Y.T. Zhu, R.Z. Valiev, Deformation behavior and plastic instabilities of ultrafine-grained titanium, Appl. Phys. Lett. 79 (5) (2001) 611–613.
[63] J. Liu, A.S. Khan, L. Takacs, C.S. Meredith, Mechanical behavior of ultrafine-grained/nanocrystalline titanium synthesized by mechanical milling plus consolidation: experiments, modeling and simulation, Int. J. Plast. 64 (0) (2015) 151–163.
[64] C.S. Meredith, A.S. Khan, Texture evolution and anisotropy in the thermo-mechanical response of UFG Ti processed via equal channel angular pressing, Int. J. Plast. 30–31 (0) (2012) 202–217.
[65] Y.M. Wang, E. Ma, Strain hardening, strain rate sensitivity, and ductility of nanostructured metals, Mater. Sci. Eng. A 375–377 (2004) 46–52.
[66] V.V. Stolyarov, Y.T. Zhu, T.C. Lowe, R.K. Islamgaliev, R.Z. Valiev, A two step SPD processing of ultrafine-grained titanium, Nanostruct. Mater. 11 (7) (1999) 947–954.
[67] V. Latysh, G. Krallics, I. Alexandrov, A. Fodor, Application of bulk nanostructured materials in medicine, Curr. Appl. Phys. 6 (2) (2006) 262–266.
[68] D.-H. Kang, T.-W. Kim, Mechanical behavior and microstructural evolution of commercially pure titanium in enhanced multi-pass equal channel angular pressing and cold extrusion, Mater. Des. 31 (Supplement 1 (0)) (2010) S54–S60.
[69] C.-Y. Hyun, H.-K. Kim, Grain size dependence of flow stress in ECAPed Ti with constant texture, Trans. Nonferrous Metals Soc. China 22 (Supplement 3 (0)) (2012) s673–s677.
[70] M. Rao, U. Chakkingal, T. Raghu, Mechanical behavior of commercial purity titanium processed by equal channel angular pressing followed by cold rolling, Trans. Indian Inst. Metals 66 (4) (2013) 357–362.
[71] K.P.S.S. Bindu, K. Smetana, A. Balakrishnan, T.N. Kim, An in vivo evaluation of ultrafine grained titanium implants, J. Mater. Sci. Technol. 25 (04) (2009) 556–560.
[72] V.L. Sordi, M. Ferrante, M. Kawasaki, T.G. Langdon, Microstructure and tensile strength of grade 2 titanium processed by equal-channel angular pressing and by rolling, J. Mater. Sci. 47 (22) (2012) 7870–7876.
[73] G. Purcek, G.G. Yapici, I. Karaman, H.J. Maier, Effect of commercial purity levels on the mechanical properties of ultrafine-grained titanium, Mater. Sci. Eng. A 528 (6) (2011) 2303–2308.